An Improved Coalition Game Approach for MIMO-NOMA Clustering Integrating Beamforming and Power Allocation

Jiefei Ding, Jun Cai, *Senior Member, IEEE*, and Changyan Yi, *Member, IEEE*

***Abstract*—The multiple-input multiple-output non-orthogonal multiple access (MIMO-NOMA) has been considered as a promising multiple access technology for the fifth generation (5G) networks to improve the system capacity and the spectral efficiency. In this paper, we propose a cluster beamforming strategy to jointly optimize beamforming vectors and power allocation coefficients for mobile users (MUs) in MIMO-NOMA clustering with the aim of reducing the total power consumption. This approach avoids the peer effect during the process of beamforming matrix calculation and can obtain a closed-form solution of beamforming strategy for multi-MU MIMO-NOMA clusters. To minimize the total power consumption, we further propose an improved coalition game approach to effectively optimize MU clustering for the large-scale MIMO networks, in which the size of a cluster is flexible. Furthermore, we discuss two different MIMO-NOMA scenarios and show that employing a NOMA power coefficient set can achieve a better performance than employing a single NOMA power coefficient for each MU in a cluster. Simulation results include the performance analysis for a single MIMO-NOMA cluster and the clustering result for a large-scale MIMO system with many MUs, which show that the proposed approach is superior than counterparts in finding the power efficient MIMO-NOMA clusters.**

***Index Terms*—MIMO-NOMA, mobile user clustering, coalition game, beamforming, power allocation.**

I. Introduction

DUE to ever-increasing wireless transmission demands and limited spectrum resources, the traditional orthogonal multiple access (OMA) approaches its bottleneck in service provisioning especially during transmission rush hours. To further improve the network capacity, non-orthogonal multiple access (NOMA) has been recently proposed as a spectral efficient multiple access technique for 5G mobile networks, which allows multiple users to share the same spectrum in a non-orthogonal way [1], [2]. In NOMA, signals for different mobile users (MUs) are superposed based on the selected power coefficients and will be transmitted through the same channel. MUs detect the desired signals by exploring the successive interference cancellation (SIC) method [3], [4]. It has been proved in [5] that a hybrid way with NOMA and OMA can greatly improve the system performance over OMA in terms of spectrum efficiency and power efficiency.

Recently, combining NOMA with multiple-input multiple-output (MIMO) technique attracts more and more research interests. The combination of MIMO and NOMA (called MIMO-NOMA) introduces advantages of both technologies and can further improve spectrum reuse efficiency [6], transmission throughputs [7], [8] and power efficiency [9]. However, MIMO-NOMA also brings some new challenges as it has to effectively coordinate the resource utilization in both space and power domains, involving MU clustering (MU group formation and decoding order selection), resource management (beamforming calculation, NOMA power allocation), and potential peer effect (i.e., the interaction of MUs in beamforming calculation). The key is how to solve a mixed integer programing problem and simplify the computation through appropriate transformations or approximations so as to design a joint optimization approach.

MU clustering is generally accompanied by resource management. In literature, most of existing researches on this problem employed either multi-stage optimization approaches or simplified models to reduce computational complexity. Specifically, in [10] and [11], MU clustering optimization and the system optimization (through resource management) were decomposed into two independent subproblems, while ignoring their inherent interactions. Moreover, the objective function of MU clustering (such as the correlation coefficient maximization or the channel gain-difference maximization) was commonly set to be different from that of the system optimization (such as sum-rate maximization or power consumption minimization), so that the overall solutions may be far from optimum. The simplified models included simplified MIMO beamforming models (e.g., considering an identity beamforming matrix [12] or selecting the beamforming vector of the cell-edge MU as the cluster beamforming vector [13]) or simplified NOMA models (e.g., fixing the cluster size and power allocation coefficient [14] or a 2-MU system [15]). However, these approaches may be ineffective for large-scale MIMO systems. To further maximize the benefits of MIMO-NOMA, a joint optimization approach should be proposed.

Unfortunately, the joint MU clustering and system optimization is NP hard, and the complexity increases incredibly with the number of MUs. By further considering the mobility and a large quantity of MUs, an optimal effective and computational efficient solution is preferred [16], [17]. Coalition game is an approach to explore players' cooperative behaviors, which has

Manuscript received February 9, 2018; revised September 12, 2018; accepted December 15, 2018. Date of publication December 25, 2018; date of current version February 12, 2019. This work was supported by the Natural Sciences and Engineering Research Council of Canada (NSERC) under Discovery and CRD Grants. The review of this paper was coordinated by Dr. Y. Xin. *(Corresponding authors: Jun Cai and Changyan Yi.)*

The authors are with the Network Intelligence and Innovation Lab (NI^{2}L), ECE, University of Manitoba, Winnipeg, MB, Canada, R3T 5V6 (e-mail: dingj345@myumanitoba.ca; jun.cai@umanitoba.ca; changyan.yi@umanitoba.ca).

This paper has supplementary downloadable material available at http://ieeexplore.ieee.org.

Digital Object Identifier 10.1109/TVT.2018.2889694

been widely employed in clustering problems [18], [19]. The framework of a coalition game to determine a stable coalition structure is based on the merge-and-split rule that no player has incentive to break away. This approach is easy to be applied and has a fast convergence rate as a distributed algorithm. Moreover, coalition game allows the size of a NOMA cluster to be flexible in MU clustering if a large quantity of MUs is considered. However, the strategy of each MU is to maximize its own utility in the traditional coalition rather than improving the system performance (the global optimization), so that the solution may not be the global optimum. By considering these issues, an improved coalition game is required to make the Pareto optimal solution close to the global optimal one.

In this paper, we consider a more general MIMO-NOMA clustering model and propose a new cluster beamforming strategy for MU clustering to minimize the total power consumption. Our main focus includes two aspects: to construct a joint optimization problem and to resolve a multi-user clustering problem. In the first aspect, we carefully design the cluster beamforming strategy to let MIMO beamforming and NOMA power allocation to be jointly optimized. Then, a closed-form optimal solution is obtained and employed on MU clustering so as to make the resource management and MU clustering to be jointly considered. For the second aspect, an improved coalition game is proposed to manage MU clustering in the large-scale system for system power minimization which is compared with the traditional one. Moreover, we consider two alternative scenarios, i.e., a power coefficient set (MIMO-NOMA1) or a single power coefficient (MIMO-NOMA2) for power allocation, and analyze their properties. By further comparing with two existing clustering approaches in literature (i.e., the channel gain-correlation based and the channel gain-difference based approaches), we show that the proposed scheme is more effective in reducing the total number of formed coalitions and the total power consumption. The main contributions of this paper are summarized as follows.

- We propose a novel cluster beamforming strategy for MIMO-NOMA and employ it under two scenarios, i.e., MIMO-NOMA1 and MIMO-NOMA2. We employ a general beamforming approach (zero-forcing beamforming) to simplify the computation of our proposed cluster beamforming strategy, so that the peer effect during MU clustering is canceled. Through equivalent transformation, the NOMA power coefficient allocation can be integrated with the beamforming calculation. Moreover, we derive an optimal decoding order which can perform better than the existing works in terms of power reduction.
- We formulate MU clustering as a coalition game due to its advantages of a distributed optimization, so that it has a fast convergence speed and the flexible cluster size. To find the optimal result for the total power consumption minimization, we further make some improvements on the traditional coalition game by following the particle swarm optimization (POS) method which adjusts the utility function for each MU towards a global optimal solution.
- We analyze three major factors that may affect the performance of a MIMO-NOMA cluster: the radius of MUs, the radius difference between two MUs, and the channel correlation coefficient. In simulations, we observe that the radius of the cell-edge MU and the real part of channel correlation coefficient are the key factors influencing power consumption. Based on this fact, we find the radius thresholds under the considered simulation environment.

The rest of this paper is organized as follows. In Section II, we review the existing researches on MIMO-NOMA clustering, which are compared with our work. In Section III, we describe MIMO-NOMA and MIMO-OMA scenarios in a single base station MIMO system and introduce the system model. The results of the cluster beamforming strategy for different scenarios and cluster sizes are derived in Section IV. MIMO-NOMA clustering approaches which include a traditional coalition game and an improved coalition game are proposed in Section V. In Section VI, simulation results are presented and discussed. Section VII concludes the paper.

Notations: $\|.\|$ and $|.|$ denote the 2-norm and the absolute value, respectively. $(.)^*$, $(.)^\dagger$ and $(.)^H$ stand for the conjugate transpose, the pseudo-inverse, and the Hermitian, respectively. $\Re(.)$ and $\Im(.)$ denote the real part and the imaginary part of a complex value, respectively. $CN(,)$ represents the complex normal distribution.

II. Related Work on MIMO-NOMA MU Clustering

In literature, there are a few researches focusing on the MIMO-NOMA mobile user (MU) clustering and power allocation. Due to high complexity, existing works in this area can be classified into two categories: simplified models or multi-stage optimization approaches. The simplified models in [13]–[15] are either heuristic or ineffective for the large-scale MIMO system, so that they cannot be applied in our considered problem. In multi-stage optimization approaches, MU clustering and system optimization are usually managed in different stages. There are two different ways to decompose a complex problem into a hierarchical structure.

In the first way, MUs were grouped in the first stage based on their channel gains, i.e., the gain-correlation based [20] or the gain-difference based [21] clustering approaches. After MU clustering, the MU group set was fixed based on an assumption that NOMA was always better than OMA. By this way, the system optimization can be conducted through adjusting power allocation coefficients or calculating beamforming vectors. However, according to our analyses, NOMA may not be always better than OMA in a MIMO system, and its performance depends on both the correlation and difference of MU's channel gains. In addition, decoupling MU clustering and the system optimization may result in the solution deviated from the optimum.

The second way is to directly optimize MU clustering to improve system performance. In the first stage, an optimization was conducted on a specific NOMA cluster to get a closed-form solution for power allocation and beamforming strategy [22]. Then, it can be applied to search for an optimal cluster set among a large quantity of MUs to maximize system performance. This approach is only applied for a fixed cluster size scenario. In [23], matching game approach was employed in MU clustering optimization for a single antenna BS network, where users and sub-channel were considered as two sets of players. This algorithm grouped MUs into limited sub-channels and maximized the total sum-rate without limitations on MU cluster size. However, in the MIMO system, all sub-channels can be allocated to all MUs simultaneously, so that the two-side matching does not applicable.

Different from all these existing works, in this paper, we consider a MIMO-NOMA optimization problem and formulate it to be a joint optimization of beamforming calculation, NOMA

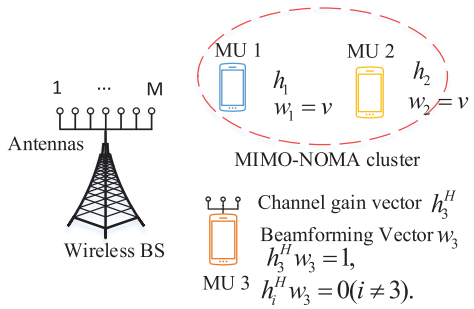

Fig. 1. A MIMO-NOMA scenario.

power allocation and MU clustering. Moreover, the cluster size is flexible and MU clustering is managed by a coalition game. Furthermore, for each stable coalition solution, we do not need to recalculate the coalition utility. To achieve the total power consumption minimum, we improve the utility function based on the result of coalition.

III. System Model

In this section, we first present the considered system model, which includes beamforming model, signal model and power model in both MIMO-OMA and MIMO-NOMA scenarios. Since these models for the different cluster sizes are only different in the dimension of vectors, we present a case of 2 MUs (mobile users) for the explanation purpose. Then, we formulate an optimization problem which includes resource management and NOMA clustering.

A. Cluster Beamforming Model

Considering a single cell downlink MIMO system, it has one base station (BS) (equipped with M antennas) and N MUs (each equipped with a single antenna), in which $M \geq N$. Let $\boldsymbol{h}_u \in R^{M\times 1}$ and $\boldsymbol{w}_u \in R^{M\times 1}$ denote the channel gain vector and beamforming vector from the BS to MU u, respectively. $\boldsymbol{W} = [\boldsymbol{w}_1, \ldots, \boldsymbol{w}_N]$ and $\boldsymbol{H} = [\boldsymbol{h}_1^T, \ldots, \boldsymbol{h}_N^T]^T$ denote the beamforming matrix and the channel gain matrix for all MUs, respectively. The difference between MIMO-OMA and MIMO-NOMA is that the orthogonal condition does not exist among MUs in the same cluster. As the example in Fig. 1, for a MU, it may have two states: served by MIMO-OMA (MO); or served MIMO-NOMA in a cluster (MN) as a cell-center user or a cell-edge user. Towards a MU in the MO state, e.g., MU_3, its beamforming vector should satisfy the orthogonal conditions (i.e., $\boldsymbol{h}_i^H \boldsymbol{w}_3 = 0$, $i \in N, i \neq 3$), and the normalized condition ($\boldsymbol{h}_3^H \boldsymbol{w}_3 = 1$). However, for MUs in a MIMO-NOMA cluster (e.g., MU_1 and MU_2), they share a same beamforming vector $\boldsymbol{v}$ which satisfies $\boldsymbol{h}_1^H \boldsymbol{v} \neq 0$, $\boldsymbol{h}_2^H \boldsymbol{v} \neq 0$ and $\boldsymbol{h}_3^H \boldsymbol{v} = 0$.

If all MUs are served by MIMO-OMA, and the beamforming matrix is calculated by the ZF-beamforming (zero-forcing beamforming) strategy [24], [25]. Because of the zero-interference condition ($\boldsymbol{h}_j^H \boldsymbol{w}_k = 0$ for $j \neq k$), the interference among MUs access to the same BS can be cancelled. Thus, we have

$$\boldsymbol{W} = \boldsymbol{H}^{\dagger} = \boldsymbol{H}^*(\boldsymbol{H}\boldsymbol{H}^*)^{-1}. \tag{1}$$

Note that beamforming vectors for all MUs are determined at the same time. Thus, a change to one MU's beamforming vector (e.g., it is grouped in a different cluster), all MUs' beamforming vectors need to be recalculated. This effect is named as the peer effect and has been ignored in most existing works. In this paper, we will show later that our proposed approach can effectively avoid such peer effects.

B. Signal Model

Let $G = \{g_1, g_2, \ldots, g_\alpha\}$ denote a set of clusters, and there are a total of α MIMO-NOMA clusters. In this set, a cluster is denoted as $g_k = \{g_{k,1}, g_{k,2}, \ldots, g_{k,n_k}\}$, where there are n_k MUs sharing the same beamforming vector and being aligned from the cell-center to the cell-edge, i.e., $g_{k,1}$ and g_{k,n_k} denote a cell-center user and a cell-edge user, respectively.

For a specific MU i in the MO state, the received signal y_i can be expressed as

$$y_i = \boldsymbol{h}_i^H \boldsymbol{w}_i^{'} \sqrt{p_i} x_i + n_i, \tag{2}$$

where $\boldsymbol{w}_i^{'} \in R^{M\times 1}$ is the beamforming vector allocated to MU i, p_i is the transmit power (Since $\|\boldsymbol{w}_i\|^2$ is unnormalized, the actual BS's power consumption is calculated as in (4)), x_i is the data symbol transmitting to MU i, and n_i denotes the additive white Gaussian noise with zero mean and variance σ_i^2. We assume $n_i/x_i^2 = \sigma^2$ for all MUs. For a guaranteed quality of service, it is required that the signal-to-interference-plus-noise ratio (SINR) at MU i is larger than a pre-determined threshold δ as

$$\gamma_i = \frac{\left|\boldsymbol{h}_i^H \boldsymbol{w}_i^{'} \sqrt{p_i}\right|^2}{\sigma^2} \geq \delta. \tag{3}$$

To meet the minimal SINR requirement, the BS' power consumption can be expressed as

$$P_i = \left\|\boldsymbol{w}_i^{'}\right\|^2 p_i = \frac{\left\|\boldsymbol{w}_i^{'}\right\|^2}{\left|\boldsymbol{h}_i^H \boldsymbol{w}_i^{'}\right|^2} \sigma^2 \delta = \left\|\boldsymbol{w}_i^{'}\right\|^2 \sigma^2 \delta. \tag{4}$$

If MU i and MU j are grouped as a MIMO-NOMA cluster k, i.e., $g_k = \{g_{k,1} = i, g_{k,2} = j\}$, the signal vector to be transmitted by the BS is given by

$$\boldsymbol{s_k} = \sqrt{p_k} \begin{bmatrix} v_{k,1}(\sqrt{\mu_{i,1}} x_i + \sqrt{\mu_{j,1}} x_j) \\ \vdots \\ v_{k,M}(\sqrt{\mu_{i,M}} x_i + \sqrt{\mu_{j,M}} x_j) \end{bmatrix}, \tag{5}$$

where $\boldsymbol{\mu_\varepsilon} = \{\sqrt{\mu_{\varepsilon,1}}, \ldots, \sqrt{\mu_{\varepsilon,M}}\}$ is the NOMA power coefficient set for signal x_ε, $\varepsilon = i, j$. On each antenna, let $\mu_{i,n} + \mu_{j,n} = 1$. Besides, the beamforming vector of the cluster k is denoted by $\boldsymbol{v_k} = \{v_{k,1}, \ldots, v_{k,M}\}$, and the transmit power is indicated by p_k. Note that in [10], MIMO-NOMA is ordinarily considered as an extension of single-antenna NOMA, so that a single power coefficient was employed to each MU on all antennas, i.e., $\mu_{i,1} = \mu_{i,2} = \cdots = \mu_{i,M}$. However, in this paper, we consider a more general case by relaxing the power coefficients on different antennas to be different [22], [26]. We term these two cases as MIMO-NOMA1 (with a power coefficient set) and MIMO-NOMA2 (with a single power coefficient).

For MIMO-NOMA1, note that NOMA employs the power coefficient set to distinguish different signals on the power domain while MIMO beamforming working the space domain. To simplify calculations, we combine the beamforming vector $\boldsymbol{v}_k$ and the power coefficient $\sqrt{\mu_{j,m}}$ to transform the original superposed transmit signal formation into a new form as shown in (6). Note that the beamforming vectors for cluster members

are different and non-orthogonal. Let

$$\boldsymbol{v_k} = \begin{bmatrix} \sqrt{p_i w_{i,1}^2 + p_j w_{j,1}^2} \\ \vdots \\ \sqrt{p_i w_{i,M}^2 + p_j w_{j,M}^2} \end{bmatrix},$$

$$\sqrt{p_k}\sqrt{\mu_{\varepsilon,m}} = \frac{\sqrt{p_\varepsilon} w_{\varepsilon,m}}{v_{k,m}} \text{ for } m \in M, \text{ and } \varepsilon = i, j.$$

The transmit signal vector can be transformed into

$$\boldsymbol{s_k} = \boldsymbol{w_i}\sqrt{p_i}x_i + \boldsymbol{w_j}\sqrt{p_j}x_j, \tag{6}$$

where the transformed beamforming vectors for MU i and MU j are denoted by $\boldsymbol{w_i}$ and $\boldsymbol{w_j}$, respectively, and the corresponding allocated power parameters are indicated by p_i and p_j. Note that $\boldsymbol{w_i}$ and $\boldsymbol{w_j}$ are different and non-orthogonal.

For MIMO-NOMA2, the transmit signal vector can be reformulated as

$$\boldsymbol{s_k} = \boldsymbol{v_k}\sqrt{p_k}(\sqrt{\mu_{i,1}}x_i + \sqrt{\mu_{j,1}}x_j). \tag{7}$$

For both cases in MIMO-NOMA, the received signal at MU ε is $y_\varepsilon = \boldsymbol{h}_\varepsilon^H \boldsymbol{s_k} + n_\varepsilon$ ($\varepsilon = i, j$), and the SINR condition (3) is applied.

C. Problem Formulation

Our objective is to minimize the total power consumption, and the system optimization problem can be formulated as

$$\min_{\boldsymbol{W},\mu,p} \sum_{i=1}^{N} P_i(\boldsymbol{w}_i, \mu_i, p_i), \tag{8a}$$

$$\text{s.t.} \quad (3) \text{ and} \tag{8b}$$

$$\boldsymbol{h}_i\boldsymbol{w}_j \begin{cases} \neq 0 \text{ If MUs } i \text{ and } j \text{ are in the same cluster,} \\ = 0 \qquad\qquad \text{Otherwise.} \end{cases} \tag{8c}$$

$$\gamma_i^j \geq \zeta\delta, \tag{8d}$$

where P_i is the power consumption for MU i (as calculated in (10) and (20)). Note that P_i is determined by the beamforming vector $\boldsymbol{w}_i$, the transmit power p_i and the power allocation coefficient μ_i (in the MN state $0 < \mu_i < 1$, and in the MO state $\mu_i = 1$). Constraint (8d) indicates that the achievable rate (or SINR) of decoding signal should be larger than a predefined threshold $\zeta\delta$ (ζ is a predefined parameter within (0, 1]) in order to ensure successful SIC decoding (refer to Appendix D) [33].

IV. Beamforming Strategy for a MIMO-NOMA Cluster

In this section, we formulate a partial ZF-beamforming problem for MIMO-NOMA clusters and introduce our cluster beamforming strategy for both MIMO-NOMA1 and MIMO-NOMA2 scenarios. In this strategy, we try to minimize the group power consumption and get the closed-form solutions. For explanation purpose, we start our discussion from the case of the 2-MU cluster, and then discuss its extension to the general multi-MU case.

A. MIMO-NOMA1 for a 2-MU Cluster

We consider MUs i and j (located from the cell-center to the cell-edge), and the pre-determined decoding order for them is in the reverse order. After decoding the superposed message, the received signals for MU i and MU j can be respectively represented as

$$\begin{aligned} y_i &= \boldsymbol{h}_i^H \boldsymbol{s_k} + n_i = \boldsymbol{h}_i^H \boldsymbol{w}_i\sqrt{p_i}x_i + n_i, \\ y_j &= \boldsymbol{h}_j^H \boldsymbol{s_k} + n_j = \boldsymbol{h}_j^H \boldsymbol{w}_j\sqrt{p_j}x_j + \boldsymbol{h}_j^H \boldsymbol{w}_i\sqrt{p_i}x_i + n_j. \end{aligned} \tag{9}$$

To meet the minimal SINR requirement, the power consumption for MU i and MU j can be respectively expressed as

$$\begin{aligned} P_i &= \|\boldsymbol{w}_i\|^2 p_i = \frac{\|\boldsymbol{w}_i\|^2}{\left|\boldsymbol{h}_i^H \boldsymbol{w}_i\right|^2}\sigma^2\delta = \|\boldsymbol{w}_i\|^2\sigma^2\delta, \\ P_j &= \|\boldsymbol{w}_j\|^2 p_j = \frac{\|\boldsymbol{w}_j\|^2}{\left|\boldsymbol{h}_j^H w_j\right|^2}(\left|\boldsymbol{h}_j^H \boldsymbol{w}_i\right|^2 p_i + \sigma^2)\delta \\ &= \|\boldsymbol{w}_j\|^2(\left|\boldsymbol{h}_j^H \boldsymbol{w}_i\right|^2 p_i + \sigma^2)\delta. \end{aligned} \tag{10}$$

A basic condition for forming a MIMO-NOMA cluster is that its total power consumption is lower than that before clustering. According to (4), if MU i and MU j are both in the MO state, the total power consumption is

$$P_i^{'} + P_j^{'} = \left\|\boldsymbol{w}_i^{'}\right\|^2\sigma^2\delta + \left\|\boldsymbol{w}_j^{'}\right\|^2\sigma^2\delta, \tag{11}$$

where $\boldsymbol{w}_i^{'}$ and $\boldsymbol{w}_j^{'}$ are the beamforming vectors in the MO state and can be directly obtained by (1). The power reduction by adopting MIMO-NOMA can be calculated by

$$\begin{aligned} \Delta P_k &= P_i^{'} + P_j^{'} - (P_i + P_j) \\ &= \left\|\boldsymbol{w}_i^{'}\right\|^2\sigma^2\delta + \left\|\boldsymbol{w}_j^{'}\right\|^2\sigma^2\delta \\ &\quad - (\|\boldsymbol{w}_i\|^2\sigma^2\delta + \|\boldsymbol{w}_j\|^2(\left|\boldsymbol{h}_j^H \boldsymbol{w}_i\right|^2 p_i + \sigma^2)\delta). \end{aligned} \tag{12}$$

By considering the possible computing cost for NOMA as Ω, we set $\Delta P_k > \Omega$ (e.g., $\Omega = 0.01w$) as the condition for a beneficial MIMO-NOMA cluster. Obviously, if $\Delta P_k < \Omega$, a NOMA cluster k will not be formed. To maximize ΔP_k, the optimal beamforming vectors can be derived based on the following optimization problem

$$\min f(\boldsymbol{w}_i, \boldsymbol{w}_j) = \|\boldsymbol{w}_i\|^2 + \|\boldsymbol{w}_j\|^2(\left|\boldsymbol{h}_j^H \boldsymbol{w}_i\right|^2\delta + 1). \tag{13}$$

According to ZF-beamforming strategy, the beamforming vectors of MUs in a cluster should be orthogonal with all out-of-cluster MUs' channel gains, but non-orthogonal with those of MUs inside this cluster. Let $\boldsymbol{H} = [\boldsymbol{h}_i^T, \boldsymbol{h}_j^T, \boldsymbol{h}_1^T, ...\boldsymbol{h}_N^T]^T \in R^{N\times M}$ be a reorganized channel gain matrix and $\boldsymbol{W} = [\boldsymbol{w}_i, \boldsymbol{w}_j, \boldsymbol{w}_1, ...\boldsymbol{w}_N] \in R^{M\times N}$ be the beamforming matrix. Then, we have

$$\begin{aligned} \boldsymbol{HW} &= \left[\boldsymbol{h}_i^T \boldsymbol{h}_j^T \boldsymbol{h}_1^T \ldots \boldsymbol{h}_N^T\right]^T \left[\boldsymbol{w}_i \boldsymbol{w}_j \boldsymbol{w}_1 \ldots \boldsymbol{w}_N\right] \\ &= \begin{bmatrix} 1 & \lambda & \boldsymbol{0}_{2\times(N-2)} \\ \beta & 1 & \\ \boldsymbol{0}_{(N-2)\times 2} & \boldsymbol{I}_{(N-2)\times(N-2)} \end{bmatrix}_{N\times N} = \boldsymbol{T}, \end{aligned} \tag{14}$$

where β and λ are two non-zero parameters denoting the non-orthogonal relationship within a cluster [26]. From the definition of beamforming matrix in the MO state $\boldsymbol{W}^{'}$ as determined in (1), we have

$$\boldsymbol{W} = \boldsymbol{H}^*(\boldsymbol{H}\boldsymbol{H}^*)^{-1}\boldsymbol{H}\boldsymbol{W} = \boldsymbol{W}^{'}\boldsymbol{T}. \tag{15}$$

From (15), we notice that beamforming vectors for a NOMA cluster is actually in a linear space expanded by the related beamforming vectors in the MO state ($\boldsymbol{w}_i^{'}$ and $\boldsymbol{w}_j^{'}$), i.e., $\boldsymbol{w}_i = \boldsymbol{w}_i^{'} + \beta\boldsymbol{w}_j^{'}$ and $\boldsymbol{w}_j = \boldsymbol{w}_j^{'} + \lambda\boldsymbol{w}_i^{'}$. Thus, one of our most

important observations is that the cluster beamforming vectors in the MN state are only determined by coefficients β and λ and have no effects on other MUs' beamforming vectors. Therefore, we can avoid the peer effect.

From (15), the beamforming vector $\boldsymbol{w}_j$ of MU j in the MN state can be derived by

$$\|\boldsymbol{w}_j\|^2 = \left\|\boldsymbol{w}_j^{'}\right\|^2\beta^2 + 2\beta\boldsymbol{w}_i^{'}\boldsymbol{w}_j^{'} + \left\|\boldsymbol{w}_i^{'}\right\|^2. \tag{16}$$

For simplifying notations, in the following, we define notation $\boldsymbol{w}_i^{'}\boldsymbol{w}_j^{'}$ which equals to $\boldsymbol{w}_i^{'T}\boldsymbol{w}_j^{'}$ in the real-valued case or $\Re(\boldsymbol{w}_i^{'})\Re(\boldsymbol{w}_j^{'}) + \Im(\boldsymbol{w}_i^{'})\Im(\boldsymbol{w}_j^{'})$ in the complex-valued case. Thus, problem (13) can be transformed into an expression with only two variables (i.e., β and λ) as

$$\begin{aligned}\min f(\boldsymbol{w}_i, \boldsymbol{w}_j) = g(\lambda, \beta) = &\left(\left\|\boldsymbol{w}_j^{'}\right\|^2\beta^2 + 2\beta\boldsymbol{w}_i^{'}\boldsymbol{w}_j^{'} + \left\|\boldsymbol{w}_i^{'}\right\|^2\right)\\ &+ \left(\left\|\boldsymbol{w}_i^{'}\right\|^2\lambda^2 + 2\lambda\boldsymbol{w}_j^{'}\boldsymbol{w}_i^{'} + \left\|\boldsymbol{w}_j^{'}\right\|^2\right)\left(\delta\left(\left|\boldsymbol{h}_j^H\boldsymbol{w}_j^{'}\right|^2\beta^2\right.\right.\\ &\left.\left. + 2\beta\left|\boldsymbol{h}_j^H\boldsymbol{w}_i^{'}\right|\left|\boldsymbol{h}_j^H\boldsymbol{w}_j^{'}\right| + \left|\boldsymbol{h}_j^H\boldsymbol{w}_i^{'}\right|^2\right) + 1\right).\end{aligned} \tag{17}$$

We notice that, after NOMA decoding, the impact of MU j on MU i is eliminated. Thus, the power consumption of MU j only depends on β, and λ only appears in the second term of (17). Moreover, $\|\boldsymbol{w}_i\|^2$ and $(\left|\boldsymbol{h}_j^H\boldsymbol{w}_i\right|^2\delta + 1)$ are always larger than zero in any value of β. Therefore, $\min\|\boldsymbol{w}_j\|^2$ is the necessary condition of $\min f(\boldsymbol{w}_i, \boldsymbol{w}_j)$, and $\|\boldsymbol{w}_j\|^2$ can be regarded as an independent sub-optimization problem. We calculate the 1st and the 2nd derivatives of (17) with respect to λ. Since $\frac{\partial^2 g(\lambda,\beta)}{\partial\lambda^2} = 2\left\|\boldsymbol{w}_i^{'}\right\|^2 > 0$, $g(\lambda, \beta)$ will reach the minimal point when $\frac{\partial g(\lambda,\beta)}{\partial\lambda} = 0$, which results in $\lambda = -\frac{\boldsymbol{w}_j^{'}\boldsymbol{w}_i^{'}}{\left\|\boldsymbol{w}_i^{'}\right\|^2}$. Then, $g(\lambda, \beta)$ can be simplified as

$$\begin{aligned}g(\lambda, \beta) &= g(\beta)\\ &= \left(\left\|\boldsymbol{w}_j^{'}\right\|^2\beta^2 + 2\beta\boldsymbol{w}_i^{'}\boldsymbol{w}_j^{'} + \left\|\boldsymbol{w}_i^{'}\right\|^2\right)\\ &\quad + \|\boldsymbol{w}_j\|^2(\delta\beta^2 + 1).\end{aligned} \tag{18}$$

Similarly, since $\frac{\partial^2 g(\beta)}{\partial\beta^2} = 2(\left\|\boldsymbol{w}_j^{'}\right\|^2 + \delta\|\boldsymbol{w}_j\|^2) > 0$, by letting $\frac{\partial g(\beta)}{\partial\beta} = 0$, we have

$$\beta = \frac{-B}{2A} = \frac{-\boldsymbol{w}_i^{'}\boldsymbol{w}_j^{'}}{\left\|\boldsymbol{w}_j^{'}\right\|^2 + \delta\|\boldsymbol{w}_j\|^2} = \frac{-\left\|\boldsymbol{w}_i^{'}\right\|^2\boldsymbol{w}_i^{'}\boldsymbol{w}_j^{'}}{\left\|\boldsymbol{w}_i^{'}\right\|^2\left\|\boldsymbol{w}_j^{'}\right\|^2(1+\delta) - \delta\left|\boldsymbol{w}_i^{'}\boldsymbol{w}_j^{'}\right|^2}. \tag{19}$$

Note that, for a beneficial NOMA cluster, the decoding order is the descending order of the Euclidian 2-norm of beamforming vectors in the MO state (as shown in Appendix A). For example, if $\left\|\boldsymbol{w}_j^{'}\right\|^2 < \left\|\boldsymbol{w}_i^{'}\right\|^2$, MU_i is decoded firstly. Otherwise, we should first decode MU_j. Note that this decoding order has not been shown in any existing works and can ensure that the power reduction is maximized.

B. MIMO-NOMA1 for a Cluster With the Size Larger Than 2

We now extend our analysis to a general case, where there are more than 2 MUs in a MIMO-NOMA cluster. For analysis purpose, we consider that there are n MUs in a cluster locating from the cell-center to the cell-edge, indexed from 1 to n. In addition, the pre-determined decoding order is in the reverse order. According to (14), the beamforming vector of MU i can be calculated by $\boldsymbol{w}_i = \lambda_{i1}\boldsymbol{w}_1^{'} + \lambda_{i2}\boldsymbol{w}_2^{'} + \cdots + \lambda_{in}\boldsymbol{w}_n^{'}, i = 1, 2, ...n$ and $\lambda_{ii} = 1$. After decoding the superposed message, the received signals and corresponding power consumptions for MU i can be derived by

$$\begin{aligned}y_i &= \boldsymbol{h}_i^H\boldsymbol{w}_i\sqrt{p_i}x_i + \sum_{\epsilon=1}^{i-1}(\boldsymbol{h}_i^H\boldsymbol{w}_\epsilon\sqrt{p_\epsilon}x_\epsilon) + n_i,\\ P_i &= \|\boldsymbol{w}_i\|^2\left(\sum_{\epsilon=1}^{i-1}\left|\boldsymbol{h}_i^H\boldsymbol{w}_\epsilon\right|^2 p_\epsilon + \sigma^2\right)\delta.\end{aligned} \tag{20}$$

Specifically, the power consumptions for MUs n and $n-1$ are respectively equal to

$$\begin{aligned}P_{n-1} &= \|\boldsymbol{w}_{n-1}\|^2 p_{n-1}\\ &= \|\boldsymbol{w}_{n-1}\|^2(\lambda_{1n-1}^2 p_1 + \cdots + \lambda_{n-2n-1}^2 p_{n-2} + \sigma^2)\delta,\\ P_n &= \|\boldsymbol{w}_n\|^2 p_n = \|\boldsymbol{w}_n\|^2(\lambda_{1n}^2 p_1 + \cdots + \lambda_{n-1n}^2 p_{n-1} + \sigma^2)\delta.\end{aligned} \tag{21}$$

To determine λ_{ij}, $i, j = 1, 2, ...n$, the objective function is to minimize the overall power consumption, i.e., The objective function is denoted by

$$\min P_1 + \cdots + P_n.$$

Based on the similar observations in (17), we propose a recursive process to determine the beamforming vectors following the order from MU n to MU 1. Specifically, since the parameters from λ_{n1} to λ_{nn-1} are only related with $\|\boldsymbol{w}_n\|^2$ as power allocation p_n is positive, the first subproblem for determining MU n's beamforming vector is denoted as

$$\begin{aligned}&\min g(\lambda_{n1}, \ldots, \lambda_{nn-1}) = \|\boldsymbol{w}_n\|^2\\ &= \lambda_{n1}^2\boldsymbol{w}_1^{'2} + \cdots + \boldsymbol{w}_n^{'2} + 2\lambda_{n1}^2\lambda_{n2}^2\boldsymbol{w}_1^{'2}\boldsymbol{w}_2^{'2} + \cdots + 2\lambda_{n1}^2\boldsymbol{w}_1^{'2}\boldsymbol{w}_n^{'2}.\end{aligned}$$

The solution can be derived by letting the 1st derivatives of the objective function be zero, i.e.,

$$\begin{aligned}&[\lambda_{n1}, \lambda_{n2}, \ldots, \lambda_{nn-1}] = BA^{-1},\\ &A = \begin{bmatrix}\left\|\boldsymbol{w}_1^{'}\right\|^2 & \boldsymbol{w}_1^{'}\boldsymbol{w}_2^{'} & \cdots & \boldsymbol{w}_1^{'}\boldsymbol{w}_{n-1}^{'}\\ \boldsymbol{w}_2^{'}\boldsymbol{w}_1^{'} & \left\|\boldsymbol{w}_2^{'}\right\|^2 & \cdots & \boldsymbol{w}_2^{'}\boldsymbol{w}_{n-1}^{'}\\ \vdots & \vdots & & \vdots\\ \boldsymbol{w}_{n-1}^{'}\boldsymbol{w}_1^{'} & \boldsymbol{w}_{n-1}^{'}\boldsymbol{w}_2^{'} & \cdots & \left\|\boldsymbol{w}_{n-1}^{'}\right\|^2\end{bmatrix},\\ &B = -[\boldsymbol{w}_1^{'}\boldsymbol{w}_n^{'}, \boldsymbol{w}_2^{'}\boldsymbol{w}_n^{'}, \ldots, \boldsymbol{w}_{n-1}^{'}\boldsymbol{w}_n^{'}].\end{aligned} \tag{22}$$

After that, we substitute this solution back to the objective function, and formulate the second subproblem to determine the beamforming vector of MU $n-1$ as (based on the fact that $p_{n-1} > 0$)

$$\min g(\lambda_{n-11}, \ldots, \lambda_{n-1n}) = \|\boldsymbol{w}_{n-1}\|^2 + \|\boldsymbol{w}_n\|^2\lambda_{n-1n}^2.$$

Following the similar procedure as in (22), we can derive $\lambda_n - 1j$, $j = 1, 2, \ldots, n$. By substituting the solution back to the objective function, we can derive the subproblem for MU $n-2$. This process will be continued till all MUs have been considered.

To better illustrate this recursive solution process, we use a 3-MU cluster $g_k = \{i, j, l\}$ as an example to explain the analysis

details as follows. To meet the minimal SINR requirement, the received signal and the power consumption for MU l (which for MUs i and j are the same as in (9) and (10)) can be expressed as

$$\begin{aligned} y_l &= \boldsymbol{h}_l^H \boldsymbol{w}_l \sqrt{p_l} x_l + \sum_{\epsilon=i,j} (\boldsymbol{h}_l^H \boldsymbol{w}_\epsilon \sqrt{p_\epsilon} x_\epsilon) + n_l, \\ P_l &= \|\boldsymbol{w}_l\|^2 \left(\left| \boldsymbol{h}_l^H \boldsymbol{w}_i \right|^2 p_i + \left| \boldsymbol{h}_l^H \boldsymbol{w}_j \right|^2 p_j + \sigma^2 \right) \delta. \end{aligned} \tag{23}$$

where $p_i = \sigma^2\delta, p_j = (\left| \boldsymbol{h}_j^H \boldsymbol{w}_i \right|^2 p_i + \sigma^2)\delta$.

Similar to (14), beamforming vectors for a 3-MU NOMA cluster are determined by

$$[\boldsymbol{w}_i, \boldsymbol{w}_j, \boldsymbol{w}_l] = [\boldsymbol{w}_i^{'}, \boldsymbol{w}_j^{'}, \boldsymbol{w}_l^{'}] \begin{bmatrix} 1 & \lambda_1 & \lambda_2 \\ \lambda_3 & 1 & \lambda_4 \\ \lambda_5 & \lambda_6 & 1 \end{bmatrix}, \tag{24}$$

and the coefficients λ_ϵ ($\epsilon = 1, 2, \ldots, 6$) can be derived based on the following optimization problem to minimize the total power consumption as

$$\min g(\lambda_1, \ldots, \lambda_6) = P_i + P_j + P_l. \tag{25}$$

Starting from MU_k beamforming vector $\|\boldsymbol{w}_l\|^2$, we have

$$\begin{aligned} \min \|\boldsymbol{w}_l\|^2 = \left\| \boldsymbol{w}_i^{'} \right\|^2 \lambda_2^2 + \left\| \boldsymbol{w}_j^{'} \right\|^2 \lambda_4^2 + 2\boldsymbol{w}_i^{'} \boldsymbol{w}_j^{'} \lambda_2 \lambda_4 \\ + 2\boldsymbol{w}_i^{'} \boldsymbol{w}_l^{'} \lambda_2 + 2\boldsymbol{w}_j^{'} \boldsymbol{w}_l^{'} \lambda_4 + \left\| \boldsymbol{w}_l^{'} \right\|^2. \end{aligned} \tag{26}$$

The solution is

$$\lambda_2 = \frac{\boldsymbol{w}_j^{'} \boldsymbol{w}_l^{'} \boldsymbol{w}_i^{'} \boldsymbol{w}_j^{'} - \boldsymbol{w}_i^{'} \boldsymbol{w}_l^{'} \left\| \boldsymbol{w}_j^{'} \right\|^2}{\left\| \boldsymbol{w}_j^{'} \right\|^2 \left\| \boldsymbol{w}_i^{'} \right\|^2 - |\boldsymbol{w}_i^{'} \boldsymbol{w}_j^{'}|^2},$$

$$\lambda_4 = \frac{\boldsymbol{w}_i^{'} \boldsymbol{w}_l^{'} \boldsymbol{w}_i^{'} \boldsymbol{w}_j^{'} - \boldsymbol{w}_j^{'} \boldsymbol{w}_l^{'} \left\| \boldsymbol{w}_i^{'} \right\|^2}{\left\| \boldsymbol{w}_j^{'} \right\|^2 \left\| \boldsymbol{w}_i^{'} \right\|^2 - |\boldsymbol{w}_i^{'} \boldsymbol{w}_j^{'}|^2}.$$

Thus, we have $\boldsymbol{w}_l = \boldsymbol{w}_i^{'} \lambda_2 + \boldsymbol{w}_j^{'} \lambda_4 + \boldsymbol{w}_l^{'}$, and (25) can be transformed into

$$\begin{aligned} \min g(\lambda_1, \ldots, \lambda_6) = \left(\|\boldsymbol{w}_j\|^2 \left(\left| \boldsymbol{h}_j^H \boldsymbol{w}_i \right|^2 \delta + 1 \right) \right. \\ + \theta\delta \left| \boldsymbol{h}_l^H \boldsymbol{w}_j \right|^2 \left(\left| \boldsymbol{h}_j^H \boldsymbol{w}_i \right|^2 \delta + 1 \right) \big) \\ \left. + \left(\|\boldsymbol{w}_i\|^2 + \theta \left(\delta \left| \boldsymbol{h}_l^H \boldsymbol{w}_i \right|^2 + 1 \right) \right) \right), \end{aligned} \tag{27}$$

where $\theta = \|\boldsymbol{w}_l\|^2$. Next, we focus on $\boldsymbol{w}_j$. Since $(\left| \boldsymbol{h}_j^H \boldsymbol{w}_i \right|^2 \delta + 1) > 0$, a second sub-optimization is formulated as

$$\begin{aligned} \min \|\boldsymbol{w}_j\|^2 \alpha + \left| \boldsymbol{h}_l^H \boldsymbol{w}_j \right|^2 \beta = \alpha \left\| \boldsymbol{w}_i^{'} \right\|^2 \lambda_1^2 + (\alpha \left\| \boldsymbol{w}_l^{'} \right\|^2 + \beta) \lambda_6^2 \\ + 2\alpha \boldsymbol{w}_i^{'} \boldsymbol{w}_l^{'} \lambda_1 \lambda_6 + 2\alpha \boldsymbol{w}_i^{'} \boldsymbol{w}_j^{'} \lambda_1 + 2\alpha \boldsymbol{w}_j^{'} \boldsymbol{w}_l^{'} \lambda_6 + \alpha \left\| \boldsymbol{w}_j^{'} \right\|^2, \end{aligned} \tag{28}$$

where $\alpha = (\left| \boldsymbol{h}_j^H \boldsymbol{w}_i \right|^2 \delta + 1)$ and $\beta = \alpha\theta\delta$. We obtain

$$\lambda_1 = \frac{\boldsymbol{w}_i^{'} \boldsymbol{w}_j^{'} (\left\| \boldsymbol{w}_l^{'} \right\|^2 + \theta\delta) - \boldsymbol{w}_i^{'} \boldsymbol{w}_l^{'} \boldsymbol{w}_j^{'} \boldsymbol{w}_l^{'}}{|\boldsymbol{w}_i^{'} \boldsymbol{w}_l^{'}|^2 - \left\| \boldsymbol{w}_i^{'} \right\|^2 (\left\| \boldsymbol{w}_l^{'} \right\|^2 + \theta\delta)},$$

$$\lambda_6 = \frac{\left\| \boldsymbol{w}_i^{'} \right\|^2 \boldsymbol{w}_j^{'} \boldsymbol{w}_l^{'} - \boldsymbol{w}_i^{'} \boldsymbol{w}_j^{'} \boldsymbol{w}_i^{'} \boldsymbol{w}_l^{'}}{|\boldsymbol{w}_i^{'} \boldsymbol{w}_l^{'}|^2 - \left\| \boldsymbol{w}_i^{'} \right\|^2 (\left\| \boldsymbol{w}_l^{'} \right\|^2 + \theta\delta)},$$

and $\boldsymbol{w}_j = \boldsymbol{w}_i^{'} \lambda_1 + \boldsymbol{w}_j^{'} + \boldsymbol{w}_l^{'} \lambda_6$. With these results, problem (25) can be further simplified as

$$\begin{aligned} \min g(\lambda_1, \ldots, \lambda_6) = \|\boldsymbol{w}_i\|^2 + \left| \boldsymbol{h}_j^H \boldsymbol{w}_i \right|^2 \left(\|\boldsymbol{w}_j\|^2 \delta + \theta\delta^2 \left| \boldsymbol{h}_l^H \boldsymbol{w}_j \right|^2 \right) \\ + \theta\delta \left| \boldsymbol{h}_l^H \boldsymbol{w}_i \right|^2 = \left(\left\| \boldsymbol{w}_j^{'} \right\|^2 + \alpha^{'} \right) \lambda_3^2 + \left(\left\| \boldsymbol{w}_l^{'} \right\|^2 + \beta^{'} \right) \lambda_5^2 \\ + 2\boldsymbol{w}_j^{'} \boldsymbol{w}_l^{'} \lambda_3 \lambda_5 + 2\boldsymbol{w}_i^{'} \boldsymbol{w}_j^{'} \lambda_3 + 2\boldsymbol{w}_i^{'} \boldsymbol{w}_l^{'} \lambda_5 + \left\| \boldsymbol{w}_i^{'} \right\|^2, \end{aligned} \tag{29}$$

where $\alpha^{'} = (\left\| \boldsymbol{w}_j^{'} \right\|^2 \delta + \left| \boldsymbol{h}_l^H \boldsymbol{w}_j \right|^2 \delta^2 \theta)$, $\beta^{'} = \theta\delta$. We have

$$\lambda_3 = \frac{\boldsymbol{w}_i^{'} \boldsymbol{w}_j^{'} (\left\| \boldsymbol{w}_l^{'} \right\|^2 + \beta^{'}) - \boldsymbol{w}_i^{'} \boldsymbol{w}_l^{'} \boldsymbol{w}_j^{'} \boldsymbol{w}_l^{'}}{|\boldsymbol{w}_j^{'} \boldsymbol{w}_l^{'}|^2 - (\left\| \boldsymbol{w}_j^{'} \right\|^2 + \alpha^{'})(\left\| \boldsymbol{w}_l^{'} \right\|^2 + \beta^{'})},$$

$$\lambda_5 = \frac{\boldsymbol{w}_i^{'} \boldsymbol{w}_l^{'} (\left\| \boldsymbol{w}_j^{'} \right\|^2 + \alpha^{'}) - \boldsymbol{w}_i^{'} \boldsymbol{w}_j^{'} \boldsymbol{w}_j^{'} \boldsymbol{w}_l^{'}}{|\boldsymbol{w}_j^{'} \boldsymbol{w}_l^{'}|^2 - (\left\| \boldsymbol{w}_j^{'} \right\|^2 + \alpha^{'})(\left\| \boldsymbol{w}_l^{'} \right\|^2 + \beta^{'})},$$

and $\boldsymbol{w}_i = \boldsymbol{w}_i^{'} + \boldsymbol{w}_j^{'} \lambda_3 + \boldsymbol{w}_l^{'} \lambda_5$. In summary, the closed-form solution of beamforming strategy for a 3-MU cluster is obtained by three steps, and in each step, the optimization is linear.

C. MIMO-NOMA2 for a Cluster With a Size of 2

In MIMO-NOMA2, a same power allocation coefficient is employed for different antennas. Thus, the received signals for MU i and MU j can be represented as

$$\begin{aligned} y_i &= \boldsymbol{h}_i^H \boldsymbol{s}_{\boldsymbol{k}} + n_i = \boldsymbol{h}_i^H \boldsymbol{v}_k \sqrt{p_k} \sqrt{\mu_{i,1}} x_i + n_i, \\ y_j &= \boldsymbol{h}_j^H \boldsymbol{s}_{\boldsymbol{k}} + n_j = \boldsymbol{h}_j^H \boldsymbol{v}_k \sqrt{p_k} \sqrt{\mu_{j,1}} x_j \\ &\quad + \boldsymbol{h}_j^H \boldsymbol{v}_k \sqrt{p_k} \sqrt{\mu_{i,1}} x_i + n_j. \end{aligned} \tag{30}$$

With the minimal SINR requirement satisfied, the power consumption for them can be respectively expressed as

$$\begin{aligned} P_i &= \|\boldsymbol{v}_k\|^2 p_k \mu_{i,1} = \frac{\|\boldsymbol{v}_k\|^2}{\left| \boldsymbol{h}_i^H \boldsymbol{v}_k \right|^2} \sigma^2 \delta, \\ P_j &= \|\boldsymbol{v}_k\|^2 p_k \mu_{j,1} = \frac{\|\boldsymbol{v}_k\|^2}{\left| \boldsymbol{h}_j^H \boldsymbol{v}_{\boldsymbol{k}} \right|^2} (\left| \boldsymbol{h}_j^H \boldsymbol{v}_k \right|^2 p_k \mu_{i,1} + \sigma^2) \delta \\ &= \|\boldsymbol{v}_k\|^2 \left(\frac{\delta}{\left| \boldsymbol{h}_i^H \boldsymbol{v}_{\boldsymbol{k}} \right|^2} + \frac{1}{\left| \boldsymbol{h}_j^H \boldsymbol{v}_{\boldsymbol{k}} \right|^2} \right) \sigma^2 \delta. \end{aligned} \tag{31}$$

To minimize the total power consumption, we formulate an optimization problem as

$$\min f(\boldsymbol{v}_k) = \|\boldsymbol{v}_k\|^2 \left(\frac{\delta + 1}{\left| \boldsymbol{h}_i^H \boldsymbol{v}_{\boldsymbol{k}} \right|^2} + \frac{1}{\left| \boldsymbol{h}_j^H \boldsymbol{v}_{\boldsymbol{k}} \right|^2} \right) \sigma^2 \delta. \tag{32}$$

Since the cluster beamforming vector $\boldsymbol{v}_k$ should be orthogonal to channel gain vectors of MU l (i.e., $\boldsymbol{h}_l{}^H \boldsymbol{v}_k = 0, l \in M, l \neq \{i, j\}$), according to (14), $\boldsymbol{v}_k$ should be in the linear space determined by $\boldsymbol{w}_i^{'}$ and $\boldsymbol{w}_j^{'}$. We rewrite $\boldsymbol{v}_k$ as $\boldsymbol{v}_k = \beta \boldsymbol{w}_i^{'} + \lambda \boldsymbol{w}_j^{'}$. Then, problem (32) can also be transformed with respect to β and λ as

$$\begin{aligned} &\min g(\beta, \lambda) \\ &= \left(\left\| \boldsymbol{w}_i^{'} \right\|^2 \beta^2 + 2\beta\lambda \boldsymbol{w}_i^{'} \boldsymbol{w}_j^{'} + \left\| \boldsymbol{w}_j^{'} \right\|^2 \lambda^2 \right) \left(\frac{\delta + 1}{\beta^2} + \frac{1}{\lambda^2} \right). \end{aligned} \tag{33}$$

From (33), we notice that $g(\beta, \lambda)$ is only determined by the ratio of $\frac{\beta}{\lambda}$. Thus, without loss of generality, we assume that

$\beta = \chi\lambda$, and let $\lambda = 1$, so that $\beta = \chi$. Then, the optimization problem can be reformulated as

$$f(\boldsymbol{v}_k) = g(\chi) = \left(\left\|\boldsymbol{w}_i^{'}\right\|^2\chi^2 + 2\chi\boldsymbol{w}_i^{'}\boldsymbol{w}_j^{'} + \left\|\boldsymbol{w}_j^{'}\right\|^2\right)\left(\frac{\delta+1}{\chi^2}+1\right). \tag{34}$$

Although the optimal result of χ can be obtained by letting $\frac{\partial g(\chi)}{\partial \chi} = 0$, the closed-form solution cannot be derived directly. If the distance between two MUs in a cluster is large, the cell-edge MU will consume much more energy than the cell-center MU, i.e., $\left\|\boldsymbol{w}_i^{'}\right\|^2 \ll \left\|\boldsymbol{w}_j^{'}\right\|^2$ and $\beta \gg \lambda$, and we have $\frac{\delta+1}{\chi^2} \ll 1$. By letting $\frac{\delta+1}{\chi^2} = 0$, problem (32) can be approximated as

$$\min g(\chi) = \left(\left\|\boldsymbol{w}_i^{'}\right\|^2\chi^2 + 2\chi\boldsymbol{w}_i^{'}\boldsymbol{w}_j^{'} + \left\|\boldsymbol{w}_j^{'}\right\|^2\right). \tag{35}$$

Since $\frac{\partial^2 g(\chi)}{\partial \chi^2} = 2\left\|\boldsymbol{w}_i^{'}\right\|^2 > 0$, by letting $\frac{\partial g(\chi)}{\partial \chi} = 0$, we have the closed-form solution as $\chi = -\frac{\boldsymbol{w}_i^{'}\boldsymbol{w}_j^{'}}{\left\|\boldsymbol{w}_i^{'}\right\|^2}$. The accuracy of the approximation will be decreased as two MUs get closer. However, if two MUs are too close, condition $\Delta P_k > \theta$ may not be satisfied. In the simulation part, we will show that this approximate solution is in high-accuracy. Moreover, the result of χ for $\frac{\delta+1}{\chi^2} \geq 1$ does not exist as shown in Appendix B. In summary, for MIMO-NOMA2 scenario, we can simplify the objective function based on the fact that $\left\|\boldsymbol{w}_i^{'}\right\|^2 \ll \left\|\boldsymbol{w}_j^{'}\right\|^2$. Moreover, from (31), we have $\frac{\mu_{i,1}}{\mu_{j,1}} = \frac{\left|\boldsymbol{h}_j^H\boldsymbol{v}_{\boldsymbol{k}}\right|^2}{\delta\left|\boldsymbol{h}_j^H\boldsymbol{v}_{\boldsymbol{k}}\right|^2+\left|\boldsymbol{h}_i^H\boldsymbol{v}_{\boldsymbol{k}}\right|^2}$, then we can get the allocated power coefficients ($\mu_{i,1}$ and $\mu_{j,1}$).

D. MIMO-NOMA2 for a Cluster With the Size Large Than 2

For the cluster with n ($n > 2$) MUs, the beamforming vector of MU i can be calculated by $\boldsymbol{v}_k = \lambda_1\boldsymbol{w}_1^{'} + \lambda_2\boldsymbol{w}_2^{'} + \cdots + \lambda_n\boldsymbol{w}_n^{'}$. After decoding the superposed message and approximation, the received signals and corresponding power consumptions for MU i can be derived by

$$y_i = \boldsymbol{h}_i^H\boldsymbol{v}_k\sqrt{p_k}\left(\sqrt{\mu_{i,1}}x_i + \sum_{j=1}^{i-1}\sqrt{\mu_{j,1}}x_j\right) + n_i.$$

$$P_i = \|\boldsymbol{v}_k\|^2\left(\frac{1}{\left|\boldsymbol{h}_i^H\boldsymbol{v}_{\boldsymbol{k}}\right|^2} + \sum_{j=1}^{i-1}\frac{\delta(1+\delta)^{(i-1-j)}}{\left|\boldsymbol{h}_j^H\boldsymbol{v}_{\boldsymbol{k}}\right|^2}\right)\sigma^2\delta.$$

The objective function can be denoted as

$$\min g(\lambda_1,\ldots,\lambda_n) = \|\boldsymbol{v}_k\|^2\left(\sum_{j=1}^{i-1}\frac{(\delta+1)^{(n-j)}}{\lambda_j^2} + \frac{1}{\lambda_n^2}\right)\sigma^2\delta. \tag{36}$$

If $\frac{(\delta+1)^{(n-j)}}{\lambda_j^2}$ is the largest one, after approximation, the objective function can be transformed as

$$\min g(\lambda_1,\ldots,\lambda_n) = \|\boldsymbol{v}_k\|^2\left(\frac{(\delta+1)^{(n-j)}}{\lambda_j^2}\right)\sigma^2\delta.$$

Following the same way as in (22), we can obtain the closed form solution by

$$\left[\frac{\lambda_1}{\lambda_j},\ldots,\frac{\lambda_{j-1}}{\lambda_j},\frac{\lambda_{j+1}}{\lambda_j},\ldots,\frac{\lambda_n}{\lambda_j}\right] = -\left[\boldsymbol{w}_1^{'}\boldsymbol{w}_j^{'},\ldots,\boldsymbol{w}_n^{'}\boldsymbol{w}_j^{'}\right]\begin{bmatrix}\left\|\boldsymbol{w}_1^{'}\right\|^2 & \boldsymbol{w}_1^{'}\boldsymbol{w}_2^{'} & \cdots & \boldsymbol{w}_1^{'}\boldsymbol{w}_n^{'}\\ \boldsymbol{w}_1^{'}\boldsymbol{w}_2^{'} & \left\|\boldsymbol{w}_2^{'}\right\|^2 & \cdots & \boldsymbol{w}_2^{'}\boldsymbol{w}_n^{'}\\ \vdots & \vdots & & \vdots\\ \boldsymbol{w}_1^{'}\boldsymbol{w}_n^{'} & \boldsymbol{w}_2^{'}\boldsymbol{w}_n^{'} & \cdots & \left\|\boldsymbol{w}_n^{'}\right\|^2\end{bmatrix}^{-1}.$$

For example, in a 3-MU cluster $g_k = \{i, j, l\}$, the received signal and the power consumption for MU l (which for MUs i and j are shown in (30) and (31)) can be written as

$$\begin{aligned} y_l &= \boldsymbol{h}_l^H\boldsymbol{v}_k\sqrt{p_k}\sqrt{\mu_{l,1}}x_l + \boldsymbol{h}_l^H\boldsymbol{v}_k\sqrt{p_k}\sqrt{\mu_{i,1}}x_i \\ &\quad + \boldsymbol{h}_l^H\boldsymbol{v}_k\sqrt{p_k}\sqrt{\mu_{j,1}}x_j + n_l, \\ P_l &= \|\boldsymbol{v}_k\|^2 p_k\mu_{l,1} = \|\boldsymbol{v}_k\|^2 \\ &\quad \times\left(\frac{\delta(\delta+1)}{\left|\boldsymbol{h}_i^H\boldsymbol{v}_{\boldsymbol{k}}\right|^2} + \frac{\delta}{\left|\boldsymbol{h}_j^H\boldsymbol{v}_{\boldsymbol{k}}\right|^2} + \frac{1}{\left|\boldsymbol{h}_l^H\boldsymbol{v}_{\boldsymbol{k}}\right|^2}\right)\sigma^2\delta. \end{aligned} \tag{37}$$

Similarly, we assume that $\boldsymbol{v}_{\boldsymbol{k}} = \lambda_1\boldsymbol{w}_i + \lambda_2\boldsymbol{w}_j + \lambda_3\boldsymbol{w}_l$ and $\lambda_2 = \alpha\lambda_1$, $\lambda_3 = \beta\lambda_1$. In order to minimize the total power consumption, the optimization function is given by

$$\begin{aligned} \min g(\alpha,\beta) = &\left(\left\|\boldsymbol{w}_i^{'}\right\|^2 + \alpha^2\left\|\boldsymbol{w}_j^{'}\right\|^2 + \beta^2\left\|\boldsymbol{w}_l^{'}\right\|^2\right. \\ &\left. + 2(\alpha\boldsymbol{w}_i^{'}\boldsymbol{w}_j^{'} + \beta\boldsymbol{w}_i^{'}\boldsymbol{w}_l^{'} + \alpha\beta\boldsymbol{w}_j^{'}\boldsymbol{w}_l^{'})\right) \\ &\times\left((\delta+1)^2 + \frac{\delta+1}{\alpha^2} + \frac{1}{\beta^2}\right). \end{aligned} \tag{38}$$

In this case, problem (38) is determined by the value of α and β. Since i is the cell-center MU and l is the cell-edge MU, we have $\left\|\boldsymbol{w}_i^{'}\right\|^2 \ll \left\|\boldsymbol{w}_l^{'}\right\|^2$, $\lambda_1 \gg \lambda_3$ and $(\delta+1)^2 \ll \frac{1}{\beta^2}$. If MU j is close to MU i, we have $\frac{(\delta+1)}{\alpha^2} \ll \frac{1}{\beta^2}$. Thus, the objective function can be approximated as

$$\begin{aligned} \min g(\alpha,\beta) = &\left(\left\|\boldsymbol{w}_i^{'}\right\|^2 + \alpha^2\left\|\boldsymbol{w}_j^{'}\right\|^2 + \beta^2\left\|\boldsymbol{w}_l^{'}\right\|^2\right. \\ &\left. + 2\alpha\boldsymbol{w}_i^{'}\boldsymbol{w}_j^{'} + 2\beta\boldsymbol{w}_i^{'}\boldsymbol{w}_l^{'} + 2\alpha\beta\boldsymbol{w}_j^{'}\boldsymbol{w}_l^{'}\right)\frac{1}{\beta^2}. \end{aligned} \tag{39}$$

We first consider β as a constant, and let $\frac{\partial(g(\alpha,\beta))}{\partial\alpha} = 0$ because $\frac{\left\|\boldsymbol{w}_j^{'}\right\|^2}{\beta^2} > 0$. As $\frac{\partial^2(g(\alpha,\beta))}{\partial\alpha^2} = \frac{\left\|\boldsymbol{w}_j^{'}\right\|^2}{\beta^2} > 0$, the objective function will reach the minimum point when $\alpha = -\frac{\boldsymbol{w}_i^{'}\boldsymbol{w}_j^{'}+\boldsymbol{w}_j^{'}\boldsymbol{w}_l^{'}\beta}{\left\|\boldsymbol{w}_j^{'}\right\|^2}$. Then, substituting α to (38), it can be further simplified as

$$\begin{aligned} \min g(\beta) = &\frac{1}{\left\|\boldsymbol{w}_j^{'}\right\|^2}\left(\left(\left\|\boldsymbol{w}_j^{'}\right\|^2\left\|\boldsymbol{w}_l^{'}\right\|^2 - \left|\boldsymbol{w}_j^{'}\boldsymbol{w}_l^{'}\right|^2\right)\right. \\ &+ \frac{2\left(\left|\boldsymbol{w}_i^{'}\boldsymbol{w}_l^{'}\right|^2\left\|\boldsymbol{w}_j^{'}\right\|^2 - \left|\boldsymbol{w}_j^{'}\boldsymbol{w}_l^{'}\right|\left|\boldsymbol{w}_i^{'}\boldsymbol{w}_j^{'}\right|\right)}{\beta} \\ &\left. + \frac{\left\|\boldsymbol{w}_i^{'}\right\|^2\left\|\boldsymbol{w}_j^{'}\right\|^2 - \left|\boldsymbol{w}_i^{'}\boldsymbol{w}_j^{'}\right|^2}{\beta^2}\right). \end{aligned} \tag{40}$$

Since the second derivative is $\frac{\partial^2(g(\beta))}{\partial\beta^2} = \frac{\|\boldsymbol{w}_i'\|^2\|\boldsymbol{w}_j'\|^2 - |\boldsymbol{w}_i'\boldsymbol{w}_j'|^2}{\|\boldsymbol{w}_j'\|^2\beta^4} > 0$, $g(\beta)$ reaches the minimum point when

$$\beta = \frac{|\boldsymbol{w}_i'\boldsymbol{w}_j'|^2 - \|\boldsymbol{w}_i'\|^2\|\boldsymbol{w}_j'\|^2}{|\boldsymbol{w}_i'\boldsymbol{w}_l'|^2\|\boldsymbol{w}_j'\|^2 - |\boldsymbol{w}_j'\boldsymbol{w}_l'||\boldsymbol{w}_i'\boldsymbol{w}_j'|},$$

$$\alpha = -\frac{|\boldsymbol{w}_i'\boldsymbol{w}_j'||\boldsymbol{w}_i'\boldsymbol{w}_l'| - |\boldsymbol{w}_j'\boldsymbol{w}_l'|\|\boldsymbol{w}_i'\|^2}{|\boldsymbol{w}_i'\boldsymbol{w}_l'|^2\|\boldsymbol{w}_j'\|^2 - |\boldsymbol{w}_j'\boldsymbol{w}_l'||\boldsymbol{w}_i'\boldsymbol{w}_j'|}.$$

Otherwise, if MU j is close to MU l, we may have $\frac{(\delta+1)}{\alpha^2} > \frac{1}{\beta^2}$. The objective function can be approximated as

$$\min g(\alpha,\beta) = (\delta+1)\left(\frac{\|\boldsymbol{w}_i'\|^2}{\alpha^2} + \|\boldsymbol{w}_j'\|^2 + \frac{\beta^2\|\boldsymbol{w}_l'\|^2}{\alpha^2} + \frac{2\boldsymbol{w}_i'\boldsymbol{w}_j'}{\alpha} + \frac{2\beta\boldsymbol{w}_i'\boldsymbol{w}_l'}{\alpha^2} + \frac{2\beta\boldsymbol{w}_j'\boldsymbol{w}_l'}{\alpha}\right). \tag{41}$$

Following the same way, we can get

$$\alpha = \frac{|\boldsymbol{w}_i'\boldsymbol{w}_l'|^2 - \|\boldsymbol{w}_i'\|^2\|\boldsymbol{w}_l'\|^2}{|\boldsymbol{w}_i'\boldsymbol{w}_j'|^2\|\boldsymbol{w}_l'\|^2 - |\boldsymbol{w}_j'\boldsymbol{w}_l'||\boldsymbol{w}_i'\boldsymbol{w}_l'|},$$

$$\beta = -\frac{|\boldsymbol{w}_i'\boldsymbol{w}_j'||\boldsymbol{w}_i'\boldsymbol{w}_l'| - |\boldsymbol{w}_j'\boldsymbol{w}_l'|\|\boldsymbol{w}_i'\|^2}{|\boldsymbol{w}_i'\boldsymbol{w}_j'|^2\|\boldsymbol{w}_l'\|^2 - |\boldsymbol{w}_j'\boldsymbol{w}_l'||\boldsymbol{w}_i'\boldsymbol{w}_l'|}.$$

According to [27], the SIC approach is based on the evaluation of received signal strength which is used to determine the weight (or precoders) on each decoding layer. Such received signal strength depends on channel gains, beamforming vectors, and power distribution. In MIMO-NOMA1, the received signal strengths for different signals are distinguished by the product of the channel gain vector, the transformed beamforming vector and the power coefficient. While in MIMO-NOMA2, since the channel gains, the beamforming vectors and the power allocations are same for different users, the received signal strength for different signals can be distinguished by the power coefficients. Take a 2-MU cluster for example. In the case of MIMO-NOMA1, for MU j in (9), the precoders of x_j and x_i are determined by $\sqrt{p_j}$ and $\lambda\sqrt{p_i}$. However, in the case of MIMO-NOMA2, for MU j in (30), the precoders of x_j and x_i are determined by$\sqrt{\mu_{j,1}}$ and $\sqrt{\mu_{i,1}}$. Therefore, although different precoders are used in MIMO-NOMA1, there is no extra overhead introduced. This observation can be easily extended to a cluster with any size.

V. MIMO-NOMA Clustering Approach

Based on the aforementioned NOMA cluster beamforming design, we have two observations: i) power reduction can be achieved through MU clustering; ii) the maximum power reduction for a cluster is only related to MUs in this cluster but independent with other out-of-cluster MUs. Based on these two observations, MU clustering problem becomes a grouping problem for exploring an optimal cluster set. In this paper, a new coalition game approach is proposed to solve such grouping problem by exploring players' cooperative behaviors.

The conditions for grouping MUs together include: the potential cluster is beneficial, and MUs can be successfully decoded (refer to Appendix D) [33]. We assume that all MUs are willing to join this clustering process and try to maximize their utilities which are assigned by the BS. The utility function of MU i is evaluated by the average value of cluster power reduction ΔP_k, i.e.,

$$U_i = \begin{cases} \Delta P_k/n_k, & i \in g_k, \\ 0, & \text{Otherwise.} \end{cases} \tag{42}$$

In a traditional coalition game, the cluster with a higher power reduction will be more potentially formed. Thus, the final clustering result may be the best choice for each player (leading to Pareto optimality) but may not be the global optimal solution in terms of minimizing the total power consumption. For example, considering four MUs (A, B, C and D) in a coalition game, the potential clusters are $g_1 = \{MU_A, MU_B\}$, $g_2 = \{MU_B, MU_C\}$ and $g_3 = \{MU_C, MU_D\}$, and the achievable power reductions for them are $\Delta P_1 = \Delta P_3 = 2$, $\Delta P_2 = 3$, respectively. The Pareto optimal solution is $G = \{g_2\}$ because MU_B and MU_C will obtain the maximum utility 1.5. However, the global optimal solution is $G = \{g_1, g_3\}$ as the total power reduction is 4. Therefore, some improvement on the traditional coalition game should be proposed. By considering the fact that a global optimal solution may be obtained when both the utility of each MU and the number of formed clusters are considered. We introduce a random variable into the design of utility function as in particle swarm optimization (PSO) approach [28] to achieve a balance between the number of formed clusters and the power reduction. The newly designed utility function $U_i^*(t)$ is defined as

$$U_i^*(t) = U_i - \kappa(t)\sum_{j=1}^{n_k} U_{g_j}, \tag{43}$$

where U_i is the average group utility in (42), U_{g_j} is the average group utility of cluster member MU j before a new cluster is formed, and $\kappa(t)$ denotes an update rate. This update rate is worked for MU i only when other cluster members (such as $j \in g_k$ and $j \neq i$) are already in different clusters and with non-zero utilities. Therefore, to make MU j split from its former cluster and join a newly cluster with MU i, utility of the newly cluster should be large enough to overcome the penalty of splitting. Note that $\kappa(t)$ is critical to the optimal solution, and the traditional coalition game is a special case when $\kappa(t) = 0$. For the stability of a coalition game, $\kappa(t)$ is only updated after all MUs converge to a Pareto optimal solution. We define t as the time to update $\kappa(t)$, which follows

$$\kappa(t) = \begin{cases} \kappa(t-1) + \theta_1 rand(1)\Delta U(t), & \Delta U(t) > 0, \\ \kappa(t-1) + \theta_2 rand(1), & \text{Otherwise.} \end{cases}$$

$$\Delta U(t) = \sum_{j=1}^{N} P_j(t) - \sum_{j=1}^{N} P_j^*, \tag{44}$$

where $rand(1)$ is a random variable within 0 to 1, $P_j(t)$ is the current result of power consumption, P_j^* is the minimum power consumption resulted from the history, and θ_1 and θ_2 are two parameters related to speed. Note that the update rate depends on the difference between the optimal result and the current result, and it can adjust the utility function to escape from the local optimal result and toward the global optimal solution.

After defining the utility functions of all MUs, the merge-and-split rule is applied, which is defined as follows.

Definition 1: Consider two sets of coalitions $\mathcal{G}_A = \{MU_i^A \cup MU_{j_1}^A ... \cup MU_{j_n}^A\}$ and $\mathcal{G}_B = \{MU_i^B \cup MU_{k_1}^B ... \cup MU_{k_l}^B\}$, which are two potential coalition groups for MU_i. Here, MU_i^A means that MU i is in the coalition group A.

For MU i, if and only if its utility in group A (denoted by $U(\mathcal{G}_A)$) is larger than its utility in group B ($U(\mathcal{G}_A) > U(\mathcal{G}_B)$), the coalition $\mathcal{G}_A$ is preferred over $\mathcal{G}_B$ by *Pareto order*, denoted by $\mathcal{G}_A^{MU_i} \rhd \mathcal{G}_B^{MU_i}$.

- *Merge:* For any individual MU from i to j_n, if $\mathcal{G}_A \rhd \{MU_i, MU_{j_1}, \ldots, MU_{j_n}\}$ and $\mathcal{G}_A = \{MU_i \cup MU_{j_1}, \ldots \cup MU_{j_n}\}$, then merge $\{MU_i, MU_{j_1}, \ldots, MU_{j_n}\}$ to $\mathcal{G}_A$, denoted by $\{MU_i, MU_{j_1}, \ldots, MU_{j_n}\} \rightarrow \mathcal{G}_A$.
- *Split:* For any coalitions $\mathcal{G}_A$ and $\mathcal{G}_B$, if $\mathcal{G}_A^{MU_i} \rhd \mathcal{G}_B^{MU_i}$, then split $\mathcal{G}_A$ into $\{MU_i, MU_{j_1}, \ldots, MU_{j_n}\}$ and merge it into a new coalition $\mathcal{G}_B$, denoted by $\{\mathcal{G}_A \cup MU_{k_1} \ldots \cup MU_{k_l}^B\} \rightarrow \{\mathcal{G}_B \cup MU_{j_1} \ldots \cup MU_{j_n}\}$.

By the merge-and-split rule, a stable coalition formation result can be found as a Pareto optimal solution [29]. We notice that if a cluster can achieve the maximal power reduction, it will be a choice with the maximum utility to each cluster member, and thus it has a higher chance of being formed. The update rate $\kappa(t)$ will be changed after each iteration. Therefore, within a single iteration, if there is no cluster with the same utility, the Pareto optimal solution is unique. Moreover, we define the $\mathbb{D}_c$ stable as in [30], where the existence and convergence proof are also available in our cases. For the different iterations, the adjustment of $\kappa(t)$ may lead to the convergence on different Pareto optimal solutions. Then, we can find one solution with the minimal power consumption as the optimal solution by the following approach.

A. Initialization

Let the best result of power consumption and the update rate be initialized as $P^* = 0$ and $k(t) = 0$, respectively, when the current update time is $t = 1$.

B. Iteration

- **Step 1:** Randomly group all MUs into different clusters and employ the split-and-merge rule on each MU to form coalitions. Then, find the potential cluster and repeat coalition formation process until none of MU changes its strategy to improve the utility.
- **Step 2:** If the current total power consumption $\sum_{j=1}^{N} P_j$ is lower than P^*, record the solution and update $P^* = \sum_{j=1}^{N} P_j^*$. Then, update $\kappa(t+1)$ by (40) and let $t = t + 1$ until $t > T$.

Here T is a predefined maximum iteration depending on the number of MUs, so that $t = T$ means the end of the iteration.

VI. Numerical Results

A. Single-Cluster Performance Analysis

In this section, we evaluate the performance of a given MIMO-NOMA cluster and the proposed clustering approach. In the simulation, we first demonstrate the impact of three main factors on the NOMA clustering and ultimately the system performance in terms of power reduction. After that, we will focus on illustrating the superiority of our proposed clustering approach by comparing with two existing ones in the literature. Since MU are randomly distributed under our settings, the probability of forming a competitively large size cluster is very low (the reason will be given in Fig. 6).

Consider a single cell network with a radius of 400 m and a centrally located BS. The number of antennas at the BS is $M = 20$ or $M = 40$. The variance of Gaussian noise is $\sigma_u^2 = -135$ dBm. The SINR requirement is $\delta = 4$ dB. Similar to the existing works [31], [32], the channel model settings include: the 3GPP long term evolution (LTE) pathloss parameters ($\alpha = 3.76$ and $\beta = 10^{-14.81}$), the Rayleigh fading with zero mean and unit variance ($\Gamma_i^{(n)} \sim CN(0,1)$), a log-normal shadowing $\gamma_i \sim N(0, 8)$ dB, and the transmit antenna power gain $G = 9$ dB. The channel coefficient between MU i and the BS's mth antenna is modeled as

$$h_i^{(m)} = \Gamma_i^{(m)} \sqrt{G\beta d_i^{-\alpha} \gamma_i}, \tag{45}$$

where d_i is the radius of MU i (i.e., the distance between MU i and the BS).

For explanation purpose, we focus on a 2-MU cluster. The impacts of three factors on the performance of power reduction are analyzed: the radius of MUs, the radius difference between two MUs, and the channel correlation coefficient. We randomly generate the locations and channel gain vectors of 10 MUs, with 5 cell-center MUs locating within radius [100, 150] m, and 5 cell-edge MUs locating within radius [346, 400]m. Then, we select one cell-center MU, namely MU_1, and one cell-edge MU, namely MU_2, to form a MIMO-NOMA cluster. The correlation between these two MUs and the shadowing coefficient are fixed by $-0.2402 - 0.1579i$ and 1.4 dB, respectively. The only thing to be changed is the radius of MU_1 or MU_2 from 110 m to 350 m. The radius of them should satisfy a condition that MU_1 is always smaller than MU_2 to keep MU_1 always to be a cell-center MU compared with the location of MU_2. Simulation results for MIMO-NOMA1 and MIMO-NOMA2 are shown in Fig. 2.

Fig. 2(a) shows the variance of power reduction resulted from clustering with respect to the radius R_1 (R_2) of the cluster member MU_1 (MU_2), under the MIMO-NOMA1 scenario. To observe the variance, we select four cross section views as shown in Fig. 2(c) by fixing one MU's radius while changing the other. As shown in Figs. 2(c-1) and 2(c-2), power reduction increases with R_2 if the radius of MU_1 is given. However, given the radius of MU_2 as shown in Figs. 2(c-3) and 2(c-4), the variance of power reduction with respect to R_1 is not that obvious unless MU_2 locates at the cell edge. By comparing Figs. 2(c-2) with 2(c-4), we can see that a larger power reduction is obtained when MUs are both close to the cell edge. Therefore, for MIMO-NOMA1, we can conclude that the power reduction is mainly determined by the radius of the cell-edge MU, so that a cell-edge MU is the necessary condition to form a beneficial cluster.

These observations imply the existence of radius thresholds in separating the area of the cell-center and the cell-edge, which can be used to narrow down the searching space of beneficial NOMA clusters. To evaluate the minimal radius for a cell-edge MU, we generate a pair of MUs which include MU_1 (radius is fixed to 100 m) and MU_2 (radius changes from 100 m to 400 m). The Rayleigh fading coefficients are generated randomly with a sample quantity of 2000, while the shadowing coefficient is fixed by 1.4 dB. Simulation shows that when the radius of MU_2 is smaller than 233 m, the power reduction is less than $0.01w$ for most of channel gain correlation coefficients. Therefore, the radius threshold for a cell-edge MU can be selected by 233 m.

The simulation results in MIMO-NOMA2 is shown in Fig. 2 (b) and (d). As shown in Fig. 2(d-1), power reduction increases with R_2 if MU_1 is located at the cell center. However, different from MIMO-NOMA1, if a MIMO-NOMA2 cluster only has cell-center MUs (as the case in Fig. 2(d-3)) or cell-edge MUs

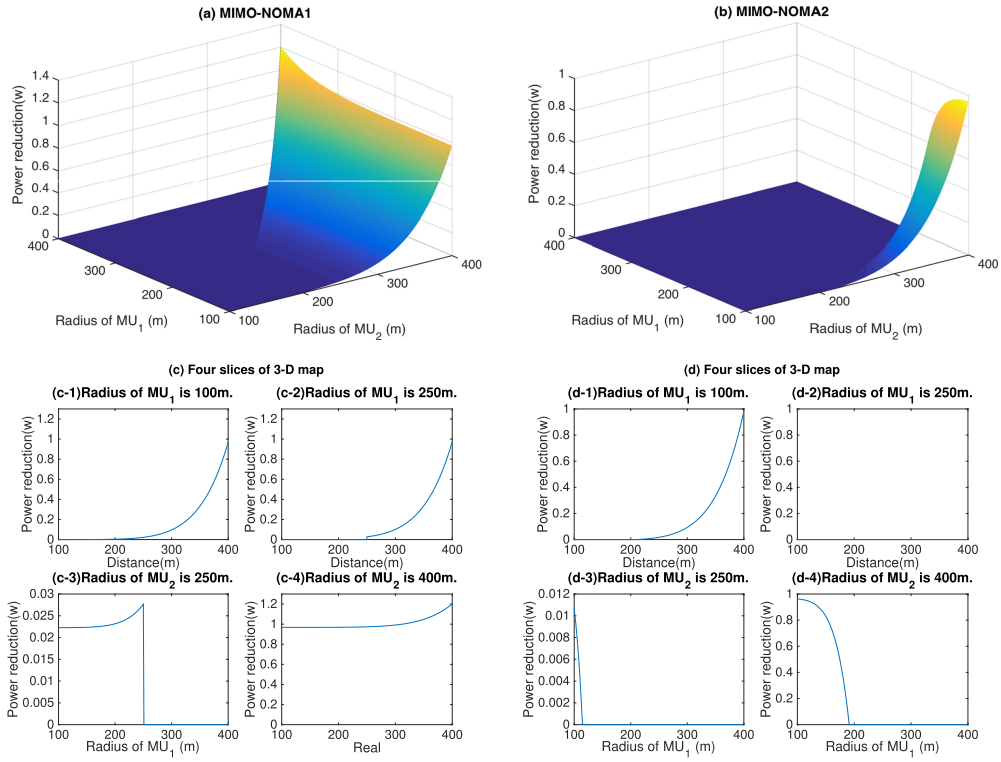

Fig. 2. 3-D map for power reduction in (a) MIMO-NOMA1 and (b) MIMO-NOMA2. (c) Four slices of 3-D map. (c-1) Radius of MU_1 is 100 m. (c-2) Radius of MU_1 is 250 m. (c-3) Radius of MU_2 is 250 m. (c-4) Radius of MU_2 is 400 m. (d) Four slices of 3-D map. (d-1) Radius of MU_1 is 100 m. (d-2) Radius of MU_1 is 250 m. (d-3) Radius of MU_2 is 250 m. (d-4) Radius of MU_2 is 400 m.

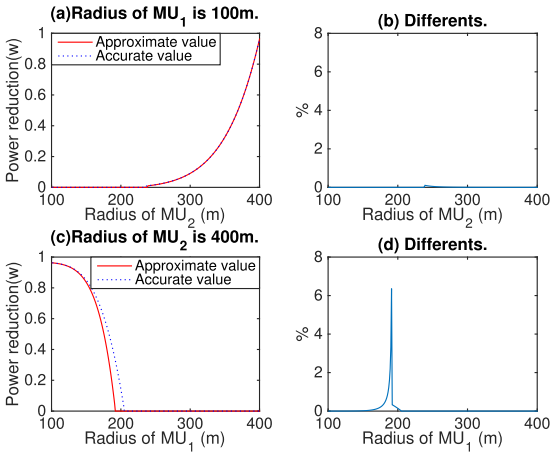

Fig. 3. Comparison, MU_1 radius is fixed in (a) and (b), MU_2 radius is fixed in (c) and (d). (a) Radius of MU_1 is 100 m. (b) Differents. (c) Radius of MU_2 is 400 m. (d) Differents.

(as shown in Fig. 2(d-2)), the power reduction is close to zero. In Fig. 2(d-4), power reduction decreases with R_1 if MU_2 is located at the cell edge. Thus, a beneficial cluster needs a cell-center MU and a cell-edge MU. In addition, by comparing Figs. 2(a) and (b), for a same pair of MUs, it is shown that MIMO-NOMA1 can achieve a better power efficiency than MIMO-NOMA2.

Since the result of MIMO-NOMA2 is an approximate solution, we have to discuss its accuracy, and show the comparison between the accurate results and the approximate ones in Fig. 3. The percentage of error is equal to the accurate result minus the approximate result and divide by the approximate result. From Figs. 3(b) and 3(d), we can observe that the approximate results are nearly the same as the accurate ones when the distance between MU_1 and MU_2 is sufficiently large. The percentage of error is less than 7% in this case. Besides, we notice that the area of the percentage of error larger than 0.1% in 3(b) (or 3(d)) is [237, 240]m (or [169, 202]m), which is a small area when compared with that lower than 0.1% [241, 400]m (or [100, 168]m). Therefore, to improve the accuracy of results, we can suitably set up radius thresholds for both cell-center MUs and cell-edge MUs and the minimum distance between them.

For obtaining the radius threshold of a cell-edge MU, the simulation process is the same as that of MIMO-NOMA1 and the radius threshold is 236 m for power reduction larger than $0.01w$. For deriving the radius threshold of a cell-center MU, we fix the radius of MU_2 as 400 m and change the radius of MU_1 from 100 m to 400 m. The results show that the radius threshold is 285 m for power reduction larger than $0.01w$. To ensure the percentage of error less than 0.1%, the minimum distance between them is 185 m. Note that since the log-normal shadowing is fixed as 1.4 under our settings, we need to consider the real log-normal shadowing value before we employing these radius threshold.

Fig. 4 shows the effects of channel gain correlation coefficient on power reduction in the vertical view, where the color in color bar from dark to light means the amount of power reduction from low to high. The channel gain correlation coefficient between MU_1 and MU_2 is a randomly generated complex value and other settings are fixed. The radius of MU_1 and MU_2 are fixed as 100 m and 400 m as shown in Figs. 4(a) and 4(b), and 100 m and

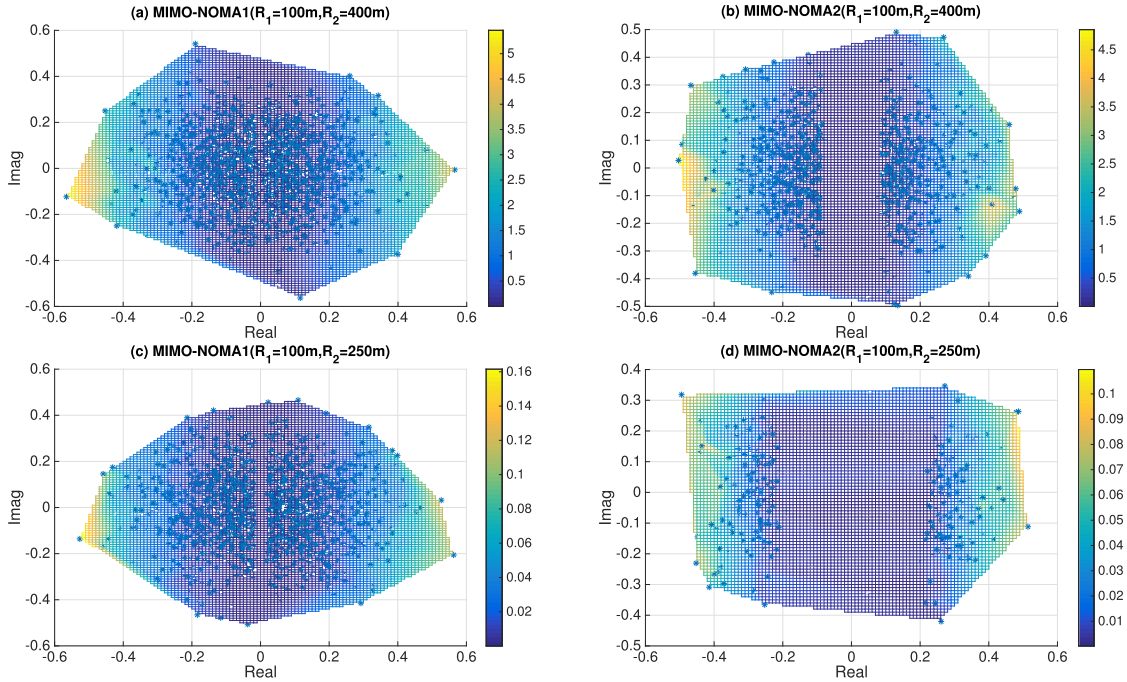

Fig. 4. Vertical view of correlation coefficient results. (a) MIMO-NOMA1($R_1 = 100$ m, $R_2 = 400$ m). (b) MIMO-NOMA2($R_1 = 100$ m, $R_2 = 400$ m). (c) MIMO-NOMA1($R_1 = 100$ m, $R_2 = 250$ m). (d) MIMO-NOMA2($R_1 = 100$ m, $R_2 = 250$ m).

270 m as shown in Figs. 4(c) and 4(d), respectively. From these figures, we can observe that the power reduction is positively associated with the absolute value of the real part of correlation coefficient while weakly associated with the imaginary part. There is a gap around zero of x-axis which indicates that if two MUs' correlation coefficient is within this gap, they can not form a beneficial NOMA cluster. We compare MIMO-NOMA1 with MIMO-NOMA2 in the same radius condition by noticing Figs. 4(a) and 4(b) or Figs. 4(c) and 4(d), and find that the gap in MIMO-NOMA1 is smaller than that in MIMO-NOMA2. It further illustrates that the solution space of MIMO-NOMA1 is larger than that of MIMO-NOMA2. Besides, by comparing Figs. 4(a) with 4(c) or Figs. 4(b) with 4(d), the gap becomes broadened, and the value of color bar is reduced, when MU_2 is getting close to the cell center. This is because R_2 has the larger influence on power reduction. The detailed explanation is in Appendix C.

B. MU Clustering Result

To evaluate the performance of our proposed MU clustering approach (power-reduction based approach), two existing approaches in literature are also simulated as benchmarks: the channel gain-correlation based approach [20] and the channel gain-difference based approach [21]. Both of them are the two-stage optimization, where MU clustering and system optimization apply independently handled. The main procedures of these two approaches are listed as follows.

1) The channel gain-correlation based approach

Step 1: Generate a metric vector $v_{i,j}$ for all MUs as

$$v_{i,j} = \begin{cases} 0 & \text{if } \left|10\log|\boldsymbol{h}_i|^2 - 10\log|\boldsymbol{h}_j|^2\right| \leq 3\,\text{dB}, \\ \left|\tilde{\boldsymbol{h}}_i \cdot \tilde{\boldsymbol{h}}_j\right|, & \text{Otherwise}, \end{cases} \tag{46}$$

where $\boldsymbol{h}_i$ and $\tilde{\boldsymbol{h}}_i$ are channel gains of MU i with and without path-loss coefficient, respectively.

Step 2: Group MUs into MIMO-NOMA clusters according to the descending order of $v_{i,j}$.

Step 3: Calculate the beamforming matrix and the power reduction. Note that the stronger user in a cluster is the MU with a larger $|\boldsymbol{h}_i|$.

2) The channel gain-difference based approach

Step 1: Generate a metric vector $\pi_{i,j}$ representing the channel gain-difference as

$$\pi_{i,j} = \begin{cases} ||\boldsymbol{h}_i| - |\boldsymbol{h}_j||, & \text{if } \frac{|\boldsymbol{h}_i \cdot \boldsymbol{h}_j|}{|\boldsymbol{h}_i||\boldsymbol{h}_j|} > 0.4, \\ 0, & \text{Otherwise}. \end{cases} \tag{47}$$

Step 2: Group MUs into MIMO-NOMA clusters according to the descending order of $\pi_{i,j}$.

Step 3: In this approach, the channel gain matrix is composed by the channel gains of MIMO-OMA MUs and the stronger MUs (i.e., with a larger $|\boldsymbol{h}_i|$) in clusters. Then, calculate the beamforming matrix and the total power reduction.

The channel gain-correlation based approach is used for MIMO-NOMA1 (denoted by MIMO-NOMA1-CO), and the channel gain-difference based approach is used for MIMO-NOMA2 (denoted by MIMO-NOMA2-GD). We further denote the proposed power-reduction based approach for MIMO-NOMA1 as MIMO-NOMA1-PO and for MIMO-NOMA2 as MIMO-NOMA2-PO, and both of them are managed by the traditional coalition game approach. In the following simulations, the BS is equipped with $M = 40$ antennas, and all MUs are distributed within a radius range of [100, 500]m. Since the different MUs' distribution and channel gains may result in a large difference on total power consumption, we compare and evaluate the system performance by a normalized average power consumption (denoted by NPC), i.e., for the result of 50 sets

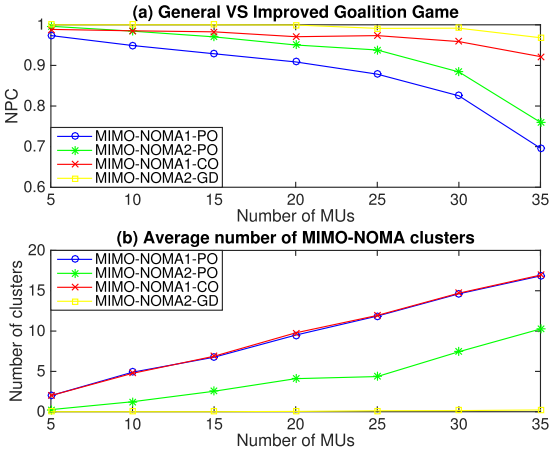

Fig. 5. Power reduction results comparison for different clustering approaches. (a) General vs. improved goalition game. (b) Average number of MIMO-NOMA clusters.

of randomly generated data, normalize them by the results of MIMO-OMA, and then calculate the average value.

From Fig. 5, we notice that the normalized power consumption is decreased with the number of MUs for all approaches. It means that NOMA-MIMO can reduce more power consumption in the large-scale system. Besides, MIMO-NOMA1 is better than MIMO-NOMA2 in improving the energy efficiency as it is more flexible on power coefficient settings. In addition, compared with the approach in literature, MIMO-NOMA1-PO (MIMO-NOMA2-PO) is better than MIMO-NOMA1-CO (MIMO-NOMA2-GD) in the scenario of MIMO-NOMA1 (MIMO-NOMA2). Thus, we can conclude that the power-reduction based approach obviously outperforms both the channel gain-correlation based and the channel gain-difference based approaches. Moreover, the performance improvement becomes more obvious with the number of MUs even in the case of the same number of MIMO-NOMA clusters as shown in Fig. 5(b). It results from the fact that the power-reduction based approach is a joint optimization approach, so that it can be more efficient in finding an optimum MIMO-NOMA cluster set than the counterparts.

The results of fixed (denoted as PO2) and flexible (denoted as PO3) cluster size conditions are compared in Fig. 6(a) and (c). For the case of fixed (or flexible) cluster size, a MIMO-NOMA cluster can only include 2 MUs (2 or 3 MUs). In this figure, MIMO-NOMA1-PO2-M1 (MIMO-NOMA2-PO3-M1) denotes the result of power-reduction based approach with fixed (flexible) cluster size condition by the traditional coalition game approach in MIMO-NOMA1 (MIMO-NOMA2) scenario. Simulation results show that the result with the flexible cluster size condition is better than without that in both MIMO-NOMA1 and MIMI-NOMA2. Besides, the difference between fixed and flexible cluster sizes are gradually increased with the number of MUs as shown in Fig. 6(c), and the difference is more obvious in MIMO-NOMA1 than MIMO-NOMA2. However, we notice that in Fig. 6(c), the difference in MIMO-NOMA1 decreases when the number of MUs is larger than 30. It means that a larger size cluster may not always be better than a smaller one in terms of average power reduction, because i) the power reduction hinges on the channel gain correlation coefficient and ii) the MU density increases with the number of MUs. In summary, MIMO-NOMA1 with the flexible cluster size condition performs better than the other cases, and the cluster size is affected by the MU density and distribution.

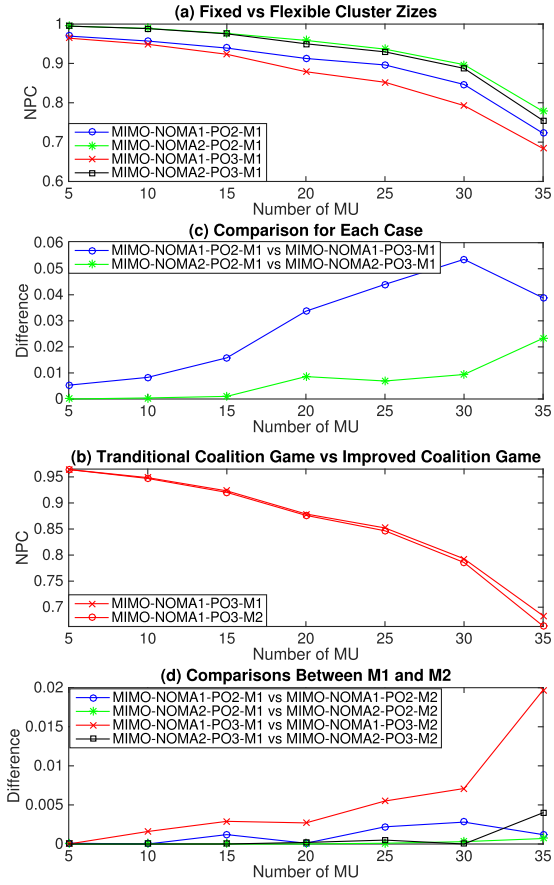

Fig. 6. Results with different cluster size limitations are shown in (a) and (c). Results for MIMO-NOMA1 with different game approaches are shown in (b) and (d). (a) Fixed vs. flexible cluster sizes. (b) Tranditional coalition game vs. improved coalition game. (c) Comparison for each case. (d) Comparisons between M1 and M2.

The results based on the improved coalition game (denoted as M2) and the traditional coalition game (denoted as M1) are compared in 6(b) and (d). In Fig. 6(b), we only compare two results between MIMO-NOMA1-PO3-M1 and MIMO-NOMA1-PO3-M2. The result of MIMO-NOMA1-PO3-M1 (MIMO-NOMA1-PO3-M2) is obtained by employing MIMO-NOMA1 with a flexible cluster size condition and operating by the traditional (improved) coalition game. We notice that the improved coalition game achieves a lower power consumption than the traditional coalition game, and such improvement has an increasing trend as the number of MUs increases. Moreover, for the case of MIMO-NOMA2 or in the fixed cluster size condition, results are in the same tendency as shown in Fig. 6(d). Furthermore, Fig. 6(d) compares M1 and M2 for 4 different cases, and the curves show the difference between them, e.g., the result of MIMO-NOMA1-PO2-M1 minus that of MIMO-NOMA1-PO2-M2. Thus, the difference means that M1 has much more power consumption than M2. In this figure, the difference value of MIMO-NOMA1 is larger than that of MIMO-NOMA2. Moreover, we observe that a small difference appears as the solution space is small (i.e., with a small quantity of MUs, or in MIMO-NOMA2 cases). Besides, we notice a significant increase in Fig. 6(d) on both MIMO-NOMA1-PO3 and MIMO-NOMA2-PO3 curves when the number of MUs is larger than 30 and

both of them have the flexible cluster size condition. Therefore, we can conclude that the improved coalition game can find a better result than the traditional coalition game approach, especially when a large quantity of MUs and the flexible cluster size condition are considered.

VII. Conclusion

In this paper, we formulate a joint optimization problem for MU clustering in the MIMO communication system to minimize the total power consumption for the BS and propose a cluster beamforming strategy to calculate the beamforming vector and power allocation coefficients for MIMO-NOMA clusters. Based on the proposed approach and the derived decoding order, a closed-form expression for cluster beamforming vector is obtained. Furthermore, we show that our proposed approach can avoid the peer effect when MUs are grouped in different clusters. Then, we carefully design an improved coalition game for MU clustering, by which the size of a NOMA cluster can be flexible and the performance of the optimal results is close to that of the global optimal solution in terms of power consumption minimization. Moreover, we compare two different MIMO-NOMA scenarios for MU clustering and find that MIMO-NOMA1 (allocated a power coefficient set for each MU) is superior than MIMO-NOMA2 (allocated a single power coefficient for each MU) in power reduction. In the simulation part, we analyze the three factors that may affect the performance of MIMO-NOMA clustering to theoretically explain that our proposed clustering approach is a high-efficient algorithm compared with other existing approaches. Furthermore, we conduct two comparisons to demonstrate that the proposed cluster beamforming strategy and the improved coalition game approach are effective in significantly improving energy efficiency for the MIMO system with a large quantity of MUs.

Appendix

A. MUs' Decoding Order

The decoding order is based on the principle that the power consumption should be minimized.

In MIMO-NOMA1, if signals are first decoded on MU_j, the optimal function is shown in (13). If signals are first decoded on MU_i, the optimal function can be rewritten as

$$f^{'}(\boldsymbol{w}_i^*, \boldsymbol{w}_j^*) = \left\|\boldsymbol{w}_j^*\right\|^2 + \|\boldsymbol{w}_i^*\|^2(\left|\boldsymbol{h}_i^H \boldsymbol{w}_j^*\right|^2\delta + 1). \tag{48}$$

By the same way, the optimal solution of (48) is $\lambda^{'} = \frac{-\left\|\boldsymbol{w}_j^{'}\right\|^2 \boldsymbol{w}_i^{'}\boldsymbol{w}_j^{'}}{\left\|\boldsymbol{w}_i^{'}\right\|^2\left\|\boldsymbol{w}_j^{'}\right\|^2(1+\delta)-\delta\left|\boldsymbol{w}_i^{'}\boldsymbol{w}_j^{'}\right|^2}$ and $\beta^{'} = -\frac{\boldsymbol{w}_j^{'}\boldsymbol{w}_i^{'}}{\left\|\boldsymbol{w}_j^{'}\right\|^2}$. If $f(\boldsymbol{w}_i, \boldsymbol{w}_j) < f^{'}(\boldsymbol{w}_i^*, \boldsymbol{w}_j^*)$, we will adopt the decoding order in (13). To compare (13) and (48), we substitute the optimal solutions into each functions and let

$$f(\boldsymbol{w}_i, \boldsymbol{w}_j) - f^{'}(\boldsymbol{w}_i^*, \boldsymbol{w}_j^*) = \frac{\delta\left|\boldsymbol{w}_i^{'}\boldsymbol{w}_j^{'}\right|^6}{(\left\|\boldsymbol{w}_i^{'}\right\|^2\left\|\boldsymbol{w}_j^{'}\right\|^2(1+\delta) - \delta\left|\boldsymbol{w}_i^{'}\boldsymbol{w}_j^{'}\right|^2)^2} \times \left(\left\|\boldsymbol{w}_i^{'}\right\|^2 - \left\|\boldsymbol{w}_j^{'}\right\|^2\right)(\delta\rho^2 - (1+\delta))(\rho^2 - 1), \tag{49}$$

where $\rho = \frac{\left|\boldsymbol{w}_i^{'}\boldsymbol{w}_j^{'}\right|}{\left\|\boldsymbol{w}_i^{'}\right\|\left\|\boldsymbol{w}_j^{'}\right\|}$. Since coefficient $\rho < 1$, $\left\|\boldsymbol{w}_i^{'}\right\|^2 < \left\|\boldsymbol{w}_j^{'}\right\|^2$ is the necessary condition for $f(\boldsymbol{w}_i, \boldsymbol{w}_j) - f^{'}(\boldsymbol{w}_i^*, \boldsymbol{w}_j^*) < 0$.

For MIMO-NOMA2, we can employ the same way to prove that the decoding order of MU_i and MU_j cannot be changed. If signals are first decoded on MU_j, we take the optimal solution $\chi = -\frac{\boldsymbol{w}_i^{'}\boldsymbol{w}_j^{'}}{\left\|\boldsymbol{w}_i^{'}\right\|^2}$ into (35) and get

$$g(\chi) = \left(\left\|\boldsymbol{w}_i^{'}\right\|^2\chi^2 + 2\chi\boldsymbol{w}_i^{'}\boldsymbol{w}_j^{'} + \left\|\boldsymbol{w}_j^{'}\right\|^2\right) = \left\|\boldsymbol{w}_j^{'}\right\|^2 - \frac{\left|\boldsymbol{w}_i^{'}\boldsymbol{w}_j^{'}\right|^2}{\left\|\boldsymbol{w}_i^{'}\right\|^2}. \tag{50}$$

If signals are first decoded on MU_i, the optimal function will be

$$\min g^{'}(\beta^*, \lambda^*) = \left(\left\|\boldsymbol{w}_i^{'}\right\|^2\chi^{*2} + 2\chi^*\boldsymbol{w}_i^{'}\boldsymbol{w}_j^{'} + \left\|\boldsymbol{w}_j^{'}\right\|^2\right) \times \left((\delta+1) + \frac{1}{\chi^{*2}}\right).$$

As the same way, we obtain $\chi^* = -\frac{\boldsymbol{w}_i^{'}\boldsymbol{w}_j^{'}}{\left\|\boldsymbol{w}_i^{'}\right\|^2}$. The minimal power consumption is

$$g^{'}(\chi^*) = (1+\delta)\left(\left\|\boldsymbol{w}_j^{'}\right\|^2 - \frac{\left|\boldsymbol{w}_i^{'}\boldsymbol{w}_j^{'}\right|^2}{\left\|\boldsymbol{w}_i^{'}\right\|^2}\right). \tag{51}$$

Thus, NOMA decoding should be always started from the MU with a maximum $\left\|\boldsymbol{w}_j^{'}\right\|^2$. For a cluster with the size larger than 2, the decoding order still need to satisfy this condition.

B. Proof for the Nonexistence of $\frac{\delta+1}{\chi^2} \geq 1$

If $\frac{\delta+1}{\chi^2} \geq 1$, the approximated problem of (34) becomes

$$\min g(\chi) = \left(\left\|\boldsymbol{w}_i^{'}\right\|^2\chi^2 + 2\chi\boldsymbol{w}_i^{'}\boldsymbol{w}_j^{'} + \left\|\boldsymbol{w}_j^{'}\right\|^2\right)\frac{\delta+1}{\chi^2} = (\delta+1)\left(\left\|\boldsymbol{w}_j^{'}\right\|^2 y^2 + 2\boldsymbol{w}_i^{'}\boldsymbol{w}_j^{'}y + \left\|\boldsymbol{w}_i^{'}\right\|^2\right). \tag{52}$$

Since $\frac{\partial^2 g(y)}{\partial y^2} = 2\left\|\boldsymbol{w}_j^{'}\right\|^2 > 0$, the result can be obtained from $\frac{\partial g(y)}{\partial y} = 0$. Thus, $\chi^* = 1/y = -\frac{\left\|\boldsymbol{w}_j^{'}\right\|^2}{\boldsymbol{w}_i^{'}\boldsymbol{w}_j^{'}}$ is the approximate solution. Comparing χ^{*2} with χ^2 in (34), we get

$$\chi^2 = \frac{(\boldsymbol{w}_i^{'}\boldsymbol{w}_j^{'})^2}{\left\|\boldsymbol{w}_i^{'}\right\|^4} = \frac{\left\|\boldsymbol{w}_j^{'}\right\|^2}{\left\|\boldsymbol{w}_i^{'}\right\|^2}\frac{(\boldsymbol{w}_i^{'}\boldsymbol{w}_j^{'})^2}{\left\|\boldsymbol{w}_i^{'}\right\|^2\left\|\boldsymbol{w}_j^{'}\right\|^2}, \qquad \chi^{*2} = \frac{\left\|\boldsymbol{w}_j^{'}\right\|^4}{(\boldsymbol{w}_i^{'}\boldsymbol{w}_j^{'})^2} = \frac{\left\|\boldsymbol{w}_j^{'}\right\|^2}{\left\|\boldsymbol{w}_i^{'}\right\|^2}\frac{\left\|\boldsymbol{w}_i^{'}\right\|^2\left\|\boldsymbol{w}_j^{'}\right\|^2}{(\boldsymbol{w}_i^{'}\boldsymbol{w}_j^{'})^2}. \tag{53}$$

Since χ^2 is based on the assumption of $\frac{\delta+1}{\chi^2} \ll 1$, χ^2 must be larger than χ^{*2}. However, this conclusion is a contrast to the fact that $\frac{(\boldsymbol{w}_i^{'}\boldsymbol{w}_j^{'})^2}{\left\|\boldsymbol{w}_i^{'}\right\|^2\left\|\boldsymbol{w}_j^{'}\right\|^2} \leq 1$. Therefore, the solution for the case of $\frac{\delta+1}{\chi^2} \geq 1$ does not exist.

C. Explanation for the Correlation Coefficient Results

Fig. 5 shows that the power reduction is mainly positive associated with the absolute value of the real part of correlation coefficient while weakly associated with the imaginary part. This is caused by the ZF-beamforming and the proposed cluster beamforming strategy. Let

$$\rho_R = \frac{\boldsymbol{w}_i^{'}\boldsymbol{w}_j^{'}}{\|\boldsymbol{w}_i^{'}\|\|\boldsymbol{w}_j^{'}\|} = \frac{(\Re(\boldsymbol{w}_i^{'})\Re(\boldsymbol{w}_j^{'}) + \Im(\boldsymbol{w}_i^{'})\Im(\boldsymbol{w}_j^{'}))}{\|\boldsymbol{w}_i^{'}\|\|\boldsymbol{w}_j^{'}\|}. \quad (54)$$

From (58) and (59), we notice that ΔP_k is positive related with ρ_R. Then, we need to prove ρ_R is mainly related with the real part of correlation coefficient R as shown in (57). According to (1), we have

$$\begin{aligned}\boldsymbol{W}^{'*}\boldsymbol{W}^{'} &= \begin{bmatrix} \|\boldsymbol{w}_1^{'}\|^2 & \boldsymbol{w}_1^{'*}\boldsymbol{w}_2^{'} \cdots & \boldsymbol{w}_1^{'*}\boldsymbol{w}_n^{'} \\ \vdots & \vdots & \vdots \\ \boldsymbol{w}_n^{'*}\boldsymbol{w}_1^{'} & \boldsymbol{w}_n^{'*}\boldsymbol{w}_2^{'} \cdots & \|\boldsymbol{w}_n^{'}\|^2 \end{bmatrix} = Q^T(\boldsymbol{H}\boldsymbol{H}^*)Q \\ &= \begin{bmatrix} \|\boldsymbol{h}_1^{'}\|^2 & \boldsymbol{h}_1^{'*}\boldsymbol{h}_2^{'} \cdots & \boldsymbol{h}_1^{'*}\boldsymbol{h}_n^{'} \\ \vdots & \vdots & \vdots \\ \boldsymbol{h}_n^{'*}\boldsymbol{h}_1^{'} & \boldsymbol{h}_n^{'*}\boldsymbol{h}_2^{'} \cdots & \|\boldsymbol{h}_n^{'}\|^2 \end{bmatrix} Q^TQ, Q = (\boldsymbol{H}\boldsymbol{H}^*)^{-1},\end{aligned}$$

where, $\boldsymbol{H}\boldsymbol{H}^*$ and Q are both symmetric matrixes, in which diagonal elements is real. Thus, Q^TQ is a real symmetric matrix. We notice that only off-diagonal elements in Q are related with the imaginary part of correlation coefficient, and which is smaller than the value of diagonal elements. Due to $\boldsymbol{w}_i^{'}\boldsymbol{w}_j^{'}$ is the real part of $\boldsymbol{w}_i^{'*}\boldsymbol{w}_j^{'}$, which is corresponding to the real part of $[\boldsymbol{h}_i^{'*}\boldsymbol{h}_1^{'}, \ldots, \boldsymbol{h}_i^{'*}\boldsymbol{h}_n^{'}]$, ρ_R is mainly related with the real part of correlation coefficient.

Here, we give a two-antenna and two-MU example as a special case for discussion. We assume that two MUs (i and j) form a MIMO-NOMA1 cluster with channel gains $[a + Bi, D + ei]$ and $[a + bi, d + ei]$, respectively. Based on (1), the beamforming vectors $\boldsymbol{w}_i^{'}$ and $\boldsymbol{w}_j^{'}$ in the OM state can be obtained by

$$\begin{cases} w_{i1}^{'} = (d-D)(ad+be)/[F^2+G^2], \\ w_{i2}^{'} = (eF-dG)/[F^2+G^2], \\ w_{i3}^{'} = (aF+bG)/[F^2+G^2], \\ w_{i4}^{'} = (b-B)(ad+be)/[F^2+G^2], \end{cases}$$
$$\begin{cases} w_{j1}^{'} = (D-d)(aD+Be)/[F^2+G^2], \\ w_{j2}^{'} = (-eF+DG)/[F^2+G^2], \\ w_{j3}^{'} = (-aF-bG)/[F^2+G^2], \\ w_{j4}^{'} = (B-b)(aD+Be)/[F^2+G^2], \end{cases} \quad (55)$$

where $F = a(d-D) + e(b-B)$ and $G = dB - bD$. The channel gain correlation coefficient between MU_1 and MU_2 (denoted by ρ), $\|\boldsymbol{w}_i^{'}\|^2$, $\left\|\boldsymbol{w}_j^{'}\right\|^2$ and $\left|\boldsymbol{w}_i^{'}\boldsymbol{w}_j^{'}\right|^2$ are calculated as

$$\begin{aligned}\rho &= \frac{(a^2+e^2+Bb+Dd)+(a(b-B)-e(d-D))i}{\sqrt{a^2+e^2+b^2+d^2}\sqrt{a^2+e^2+B^2+D^2}} \\ &= R + \frac{(a(b-B)-e(d-D))i}{\sqrt{a^2+e^2+b^2+d^2}\sqrt{a^2+e^2+B^2+D^2}}, \\ &\left\|\boldsymbol{w}_i^{'}\right\|^2 = \\ &\frac{(a^2+e^2+B^2+D^2)(a^2(d-D)^2+e^2(b-B)^2+(Bd-Db)^2)}{((a(d-D)+e(b-B))^2+(Bd-Db)^2)^2} \\ &= \frac{\|\boldsymbol{h}_j\|^2\gamma}{((a(d-D)+e(b-B))^2+(Bd-Db)^2)}, \\ &\left\|\boldsymbol{w}_j^{'}\right\|^2 = \\ &\frac{(a^2+e^2+b^2+d^2)(a^2(d-D)^2+e^2(b-B)^2+(Bd-Db)^2)}{((a(d-D)+e(b-B))^2+(Bd-Db)^2)^2} \\ &= \frac{\|\boldsymbol{h}_i\|^2\gamma}{((a(d-D)+e(b-B))^2+(Bd-Db)^2)}, \frac{\left|\boldsymbol{w}_i^{'}\boldsymbol{w}_j^{'}\right|^2}{\|\boldsymbol{w}_i^{'}\|^2\left\|\boldsymbol{w}_j^{'}\right\|^2} \\ &= \frac{R^2}{\gamma^2},\end{aligned} \quad (56)$$

where $R = \frac{(a^2+e^2+Bb+Dd)}{\sqrt{a^2+e^2+b^2+d^2}\sqrt{a^2+e^2+B^2+D^2}}$ and $\gamma = \frac{(a^2(d-D)^2+e^2(b-B)^2+(Bd-Db)^2)}{((a(d-D)+e(b-B))^2+(Bd-Db)^2)} < 1$. Note that R is the real part of correlation coefficient, γ is a variable which is related to $e(b-B)$ and $a(d-D)$. If they are equal to zero, $\|\boldsymbol{w}_i^{'}\|^2$ and $\left\|\boldsymbol{w}_j^{'}\right\|^2$ are both infinite. However, in the simulation of Fig. 4, radius of two MUs are unchanged, and channel gains in 40 antennas are generated by random valuables following $CN(0,1)$. It indicates that $\|\boldsymbol{h}_i\|^2$ and $\|\boldsymbol{h}_j\|^2$ can only be changed in a small range. Since MU j is first decoded, we have $(D^2+B^2) > (d^2+b^2)$ by condition $\|\boldsymbol{w}_i{'}\|^2 < \|\boldsymbol{w}_j{'}\|^2$. Then, we take results of λ and β into (12) as

$$\begin{aligned}\Delta P_k &= \rho_R^2\left\|\boldsymbol{w}_j^{'}\right\|^2 + \frac{\left\|\boldsymbol{w}_i^{'}\right\|^2}{\frac{1}{\rho_R^2}(1+\delta)-\delta} \\ &= R^2(\|\boldsymbol{h}_i\|^2 + \|\boldsymbol{h}_j\|^2\theta) \\ &\quad \times \frac{1}{(a^2(d-D)^2+e^2(b-B)^2+(Bd-Db)^2)}, \\ x &= \frac{\left|\boldsymbol{w}_i^{'}\boldsymbol{w}_j^{'}\right|^2}{\left\|\boldsymbol{w}_i^{'}\right\|^2\left\|\boldsymbol{w}_j^{'}\right\|^2}, \theta = \frac{x(\delta-2)+(\delta+1)}{(1+\delta-x)^2} < 1.\end{aligned} \quad (57)$$

From (58), we notice that ΔP_k is directly related to the real part of correlation coefficient R^2 while weakly related to the imaginary part of correlation coefficient through $(a^2(d-D)^2+e^2(b-B)^2+(Bd-Db)^2)$. Based on this structure, we can explain that, first of all, MIMO-NOMA1 is always better than MIMO-OMA as $\Delta P_k > 0$. However, not all

beneficial MIMO-NOMA1 cluster has $\Delta P_k > 0.01w$. Therefore, the gap in Fig. 4(c) is larger than that in Fig. 4(a) if we reduce R_2 and make $\|\boldsymbol{h}_j\|^2$ small. Second, ΔP_k increases if we increase R_1 or R_2, which can be observed from comparing the value of color bar between Fig. 4(a) and Fig. 4(c). Last, the influence of the imaginary part increases with R^2.

We conduct the same example for MIMO-NOMA2. In this case, the channel gain correlation coefficient between MU_1 and MU_2 (denoted as ρ), $\|\boldsymbol{w}_i'\|^2$ and $\left\|\boldsymbol{w}_j'\right\|^2$ are the same as in (56). Then, if we assume $\lambda = 1$ and $\beta = -\frac{\boldsymbol{w}_i'\boldsymbol{w}_j'}{\|\boldsymbol{w}_i'\|^2}$, the cluster beamforming vector $\|\boldsymbol{v}_k\|^2$ and power reduction can be calculated as

$$\begin{aligned}\|\boldsymbol{v}_k\|^2 &= \left\|\boldsymbol{w}_j'\right\|^2 - \frac{\left|\boldsymbol{w}_i'\boldsymbol{w}_j'\right|^2}{\left\|\boldsymbol{w}_i'\right\|^2},\\ \Delta P_k &= \left\|\boldsymbol{w}_j'\right\|^2\rho_R^2 + \left\|\boldsymbol{w}_i'\right\|^2\left(\delta + 2 - \frac{\delta+1}{\rho_R^2}\right)\\ &= \frac{\sigma^2\delta}{(a^2(d-D)^2 + e^2(b-B)^2 + (Bd-Db)^2)}\\ &\quad\times\left(\frac{R^2}{\gamma}\|\boldsymbol{h}_i\|^2 + \left((2+\delta)\gamma - (1+\delta)\gamma\frac{\gamma^2}{R^2}\right)\|\boldsymbol{h}_j\|^2\right).\end{aligned} \tag{58}$$

Note that if $((2+\delta)\gamma - (1+\delta)\gamma\frac{\gamma^2}{R^2}) > 0$, we have $\frac{\gamma^2}{R^2} < 2$ which makes $\rho > 1/\sqrt{2}$. In Fig. 4(b), since $\rho < 0.6$, we have $\frac{\gamma^2}{R^2} > 2$ and $((2+\delta)\gamma - (1+\delta)\gamma\frac{\gamma^2}{R^2}) < -\delta\gamma$. Moreover, since $\frac{R^2}{\gamma} < \gamma < 1$ and $\delta > 1$, $\|\boldsymbol{h}_i\|^2$ should be larger than $\|\boldsymbol{h}_j\|^2$ to make $\Delta P_k > 0$, which indicates that a beneficial MIMO-NOMA2 cluster should include both a cell-center MU and a cell-edge MU. Furthermore, if we increase $|R|$, ΔP_k will be increased more efficiently than that when we decrease γ. For the case of a cluster with the size larger than 2, according to (26), we will have

$$\left\|\boldsymbol{w}_l'\right\|^2 - \|\boldsymbol{w}_l\|^2 = \left\|\boldsymbol{w}_l'\right\|^2\frac{1+\rho_R^2}{1-\rho_R^2}(\rho_{R2}^2 + \rho_{R3}^2 - 2\rho_R\rho_{R2}\rho_{R3}). \tag{59}$$

where, ρ_{R2} (ρ_{R3}) is calculated as the same formula in (54) between i and l (j and l).

D. SIC Decoding Conditions

The achievable rate (or SINR) should be larger than a predefined threshold $\zeta\delta$ in order to ensure successful SIC decoding [33]. We transform (8d) into a constraint which can be judged by power coefficients.

For MIMO-NOMA1, the condition to make x_j successfully decode on MU i is that $\gamma_i^j > \zeta\delta = \zeta\gamma_i$. Through taking the beamforming results into this inequality, we will have $\lambda^2 > (1+\delta)\zeta$ in a 2-MU cluster. Similarly, for an n-MU cluster, if $i, j \in \{1, 2, \ldots, n\}$ and $i < j$, the signal from MU $j-1$ (and j) will be decoded at MU i, and the SINR after SIC operation can be denoted as

$$\begin{aligned}\gamma_i^{j-1} &= \frac{\left|\boldsymbol{h}_i^H\boldsymbol{w}_{j-1}\sqrt{p_{j-1}}\right|^2}{\left(\sum_{\epsilon=1}^{j-2}\left|\boldsymbol{h}_i^H\boldsymbol{w}_\epsilon\sqrt{p_\epsilon}\right|^2 + \sigma^2\right)},\\ \gamma_i^j &= \frac{\left|\boldsymbol{h}_i^H\boldsymbol{w}_j\sqrt{p_j}\right|^2}{\left(\sum_{\epsilon=1}^{j-1}\left|\boldsymbol{h}_i^H\boldsymbol{w}_\epsilon\sqrt{p_\epsilon}\right|^2 + \sigma^2\right)},\\ &= \frac{\left|\boldsymbol{h}_i^H\boldsymbol{w}_j\sqrt{p_j}\right|^2}{\left(\frac{1}{\gamma_i^{j-1}}+1\right)\left|\boldsymbol{h}_i^H\boldsymbol{w}_{j-1}\sqrt{p_{j-1}}\right|^2} > \frac{\left|\boldsymbol{h}_i^H\boldsymbol{w}_j\right|^2}{\left|\boldsymbol{h}_i^H\boldsymbol{w}_{j-1}\right|^2}\frac{\gamma_i^{j-1}}{1+\gamma_i^{j-1}}.\end{aligned}$$

Therefore, if $\gamma_i^j > \gamma_i^{j-1}$, we have $\left|\boldsymbol{h}_i^H\boldsymbol{w}_j\right|^2 > (1+\gamma_i^{j-1})\left|\boldsymbol{h}_i^H\boldsymbol{w}_{j-1}\right|^2$ for any $i+2 < j < n$. If $\gamma_i^j > \zeta\delta$, we have $\left|\boldsymbol{h}_i^H\boldsymbol{w}_j\right|^2 > \zeta\delta(1+\frac{1}{\gamma_i^{j-1}})\left|\boldsymbol{h}_i^H\boldsymbol{w}_{j-1}\right|^2$. Then, we observe that

$$\begin{aligned}\gamma_i &= \frac{p_i}{\left(\sum_{\epsilon=1}^{i-1}\left|\boldsymbol{h}_j^H\boldsymbol{w}_\epsilon\sqrt{p_\epsilon}\right|^2 + \sigma^2\right)} = \delta,\\ \gamma_i^{i+1} &= \frac{\left|\boldsymbol{h}_i^H\boldsymbol{w}_{i+1}\sqrt{p_{i+1}}\right|^2}{\left(p_i + \sum_{\epsilon=1}^{i-1}\left|\boldsymbol{h}_j^H\boldsymbol{w}_\epsilon\sqrt{p_\epsilon}\right|^2 + \sigma^2\right)},\\ &= \frac{\left|\boldsymbol{h}_i^H\boldsymbol{w}_{i+1}\sqrt{p_{i+1}}\right|^2}{p_i\left(1+\frac{1}{\delta}\right)} > \frac{\left|\boldsymbol{h}_i^H\boldsymbol{w}_{i+1}\right|^2}{\left(1+\frac{1}{\delta}\right)} > \zeta\delta.\end{aligned}$$

Therefore, we have $\left|\boldsymbol{h}_i^H\boldsymbol{w}_{i+1}\right|^2 > (1+\delta)\zeta$. Taking a 3-MU cluster for example, the condition for successful decoding is that $(1+\delta)\zeta < \lambda_4^2, \lambda_1^2$ and $\lambda_1^2(1+\frac{1}{\gamma_i^\epsilon})\zeta\delta < \lambda_2^2$.

For MIMO-NOMA2, the condition for successful decoding is that $\frac{\mu_{\epsilon+1}}{\mu_\epsilon} > \min\{\zeta\delta(1+\frac{1}{\gamma_1^\epsilon}), \ldots, \zeta\delta(1+\frac{1}{\gamma_{\epsilon-1}^\epsilon}), \zeta(1+\delta)\}$.

REFERENCES

[1] L. Dai, B. Wang, Y. Yuan, S. Han, C.-L. I, and Z. Wang, "Non-orthogonal multiple access for 5G: Solutions, challenges, opportunities, and future research trends," *IEEE Commun. Mag.*, vol. 53, no. 9, pp. 74–81, Sep. 2015.

[2] M. Zeng, A. Yadav, O. A. Dobre, G. I. Tsiropoulos, and H. V. Poor, "Capacity comparison between MIMO-NOMA and MIMO-OMA with multiple users in a cluster," *IEEE J. Sel. Areas Commun.*, vol. 35, no. 10, pp. 2413–2424, Oct. 2017.

[3] L. Lv, Q. Ni, Z. Ding, and J. Chen, "Application of non-orthogonal multiple access in cooperative spectrum-sharing networks over Nakagami-m fading channels," *IEEE Trans. Veh. Technol.*, vol. 66, no. 6, pp. 5506–5511, Jun. 2017.

[4] S. M. R. Islam, M. Zeng, O. A. Dobre, and K. S. Kwak, "Resource allocation for downlink NOMA systems: Key techniques and open issues," *IEEE Wireless Commun.*, vol. 25, no. 2, pp. 40–47, Apr. 2018.

[5] L. Song, Y. Li, Z. Ding, and H. V. Poor, "Resource management in non-orthogonal multiple access networks for 5G and beyond," *IEEE Netw.*, vol. 31, no. 4, pp. 8–14, Jul./Aug. 2017.

[6] A. J. Paulraj, D. A. Gore, R. U. Nabar, and H. Bolcskei, "An overview of MIMO communications—A key to gigabit wireless," *Proc. IEEE*, vol. 92, no. 2, pp. 198–218, Feb. 2004.

[7] W. Cai, C. Chen, L. Bai, Y. Jin, and J. Choi, "User selection and power allocation schemes for downlink NOMA systems with imperfect CSI," in *Proc. IEEE Veh. Technol. Conf.*, 2016, pp. 1–5.

[8] N. Zabetian, M. Baghani, and A. Mohammadi, "Rate optimization in NOMA cognitive radio networks," in *Proc. 8th Inter. Symp. Telecommun.*, 2016, pp. 62–65.

[9] H. Q. Tran, P. Q. Truong, C. V. Phan, and Q. T. Vien, "On the energy efficiency of NOMA for wireless backhaul in multi-tier heterogeneous cran," in *Proc. Inter. Conf. Recent Advances Signal Process, Telecommun. Comput.*, 2017, pp. 229–234.

[10] Z. Ding, R. Schober, and H. V. Poor, "A general MIMO framework for NOMA downlink and uplink transmission based on signal alignment," *IEEE Trans. Wireless Commun.*, vol. 15, no. 6, pp. 4438–4454, Jun. 2016.
[11] S. M. R. Islam, N. Avazov, O. A. Dobre, and K. S. Kwak, "Power-domain non-orthogonal multiple access (NOMA) in 5G systems: Potentials and challenges," *Commun. Surveys Tuts.*, vol. 66, no. 99, pp. 1–1, 2016.
[12] Z. Ding, F. Adachi, and H. V. Poor, "The application of MIMO to non-orthogonal multiple access," *IEEE Trans. Wireless Commun.*, vol. 15, no. 1, pp. 537–552, Jan. 2016.
[13] Q. Sun, S. Han, Z. Xu, S. Wang, I. Chih-Lin, and Z. Pan, "Sum rate optimization for MIMO non-orthogonal multiple access systems," in *Proc. IEEE Wireless Commun. Netw. Conf.*, 2015, pp. 747–752.
[14] Y. Liu, M. Elkashlan, Z. Ding, and G. K. Karagiannidis, "Fairness of user clustering in MIMO non-orthogonal multiple access systems," *IEEE Commun. Lett.*, vol. 20, no. 7, pp. 1465–1468, Jul. 2016.
[15] Z. Chen and X. Dai, "Med precoding for multi-user MIMO-NOMA downlink transmission," *IEEE Trans. Veh. Technol.*, vol. 66, no. 99, pp. 1–1, Jun. 2016.
[16] Y. F. Liu, Y. H. Dai, and Z. Q. Luo, "Coordinated beamforming for MISO interference channel: Complexity analysis and efficient algorithms," *IEEE Trans. Signal Process.*, vol. 59, no. 3, pp. 1142–1157, Mar. 2011.
[17] S. Cui, A. J. Goldsmith, and A. Bahai, "Energy-efficiency of MIMO and cooperative MIMO techniques in sensor networks," *IEEE J. Sel. Areas Commun.*, vol. 22, no. 6, pp. 1089–1098, Aug. 2004.
[18] L. Al-Kanj, Z. Dawy, W. Saad, and E. Kutanoglu, "Energy-aware cooperative content distribution over wireless networks: Optimized and distributed approaches," *IEEE Trans. Veh. Technol.*, vol. 62, no. 8, pp. 3828–3847, Oct. 2013.
[19] D. Wu, Y. Cai, and J. Wang, "A coalition formation framework for transmission scheme selection in wireless sensor networks," *IEEE Trans. Veh. Technol.*, vol. 60, no. 6, pp. 2620–2630, Jul. 2011.
[20] J. Kim, J. Koh, J. Kang, K. Lee, and J. Kang, "Design of user clustering and precoding for downlink non-orthogonal multiple access (NOMA)," in *Proc. IEEE Military Commun. Conf.*, 2015, pp. 1170–1175.
[21] B. Kimy *et al.*, "Non-orthogonal multiple access in a downlink multiuser beamforming system," in *Proc. IEEE Military Commun. Conf.*, 2013, pp. 1278–1283.
[22] J. Choi, "Minimum power multicast beamforming with superposition coding for multiresolution broadcast and application to NOMA systems," *IEEE Trans. Commun.*, vol. 63, no. 3, pp. 791–800, Mar. 2015.
[23] B. Di, L. Song, and Y. Li, "Sub-channel assignment, power allocation, and user scheduling for non-orthogonal multiple access networks," *IEEE Trans. Wireless Commun.*, vol. 15, no. 11, pp. 7686–7698, Nov. 2016.
[24] T. Yoo and A. Goldsmith, "On the optimality of multiantenna broadcast scheduling using zero-forcing beamforming," *IEEE J. Sel. Areas Commun.*, vol. 24, no. 3, pp. 528–541, Mar. 2006.
[25] B. Farhang-Boroujeny, Q. Spencer, and L. Swindlehurst, "Layering techniques for space-time communication in multi-user networks," in *Proc. IEEE Veh. Technol. Conf.*, vol. 2, 2003, pp. 1339–1343.
[26] J. Ding and J. Cai, "Efficient MIMO-NOMA clustering integrating joint beamforming and power allocation," in *Proc. IEEE GLOBECOM Conf.*, 2017.
[27] M. Fabbri, M. Chiani, and A. Giorgetti, "Introducing erasures in MIMO with successive interference cancellation to reduce error propagation," in *Proc. IEEE Int. Conf. Ultra-Wideband*, 2009, pp. 312–315.
[28] J. Kennedy, "Particle swarm optimization," in *Encyclopedia of Mach. Learning*. Berlin, Germany: Springer, 2011, pp. 760–766.
[29] S. Mathur, L. Sankar, and N. B. Mandayam, "Coalitions in cooperative wireless networks," *IEEE J. Sel. Areas Commun.*, vol. 26, no. 7, pp. 1104–1115, Sep. 2008.
[30] Z. Han, *Game Theory in Wireless and Communication Networks: Theory, Models, and Applications*. Cambridge, U.K.: Cambridge Univ. Press, 2012.
[31] A. Papadogiannis and G. C. Alexandropoulos, "The value of dynamic clustering of base stations for future wireless networks," in *Proc. IEEE World Congr. Comput. Intell.*, 2010, pp. 1–6.
[32] A. Papadogiannis, H. J. Bang, D. Gesbert, and E. Hardouin, "Efficient selective feedback design for multicell cooperative networks," *IEEE Trans. Veh. Technol.*, vol. 60, no. 1, pp. 196–205, Jan. 2011.
[33] Y. Zhou, V. W. S. Wong, and R. Schober, "Dynamic decode-and-forward based cooperative NOMA with spatially random users," *IEEE Trans. Wireless Commun.*, vol. 17, no. 5, pp. 3340–3356, May 2018.

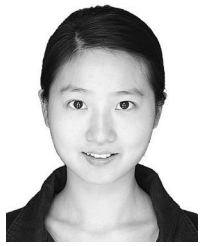

Jiefei Ding received the B.Sc. degree from Xiangtan University, Xiangtan, China, in 2012, and the M.Sc. degree from the Guangdong University of Technology, Guangzhou, China, in 2015. She is currently working toward the Ph.D. degree at the University of Manitoba, Winnipeg, MB, Canada. She visited Hong Kong University of Science and Technology as a postgraduate visiting internship student in 2015. Her research interests include game theory, resource management of cloud computing, C-RAN, MIMO, and NOMA technologies in 5G networks. She received the Best Paper Award from INISCOM in 2015.

Jun Cai (M'04–SM'14) received the B.Sc. and the M.Sc. degrees from Xi'an Jiaotong University, Xi'an, China, in 1996 and 1999, respectively, and the Ph.D. degree from the University of Waterloo, Waterloo, ON, Canada, in 2004. From June 2004 to April 2006, he was with McMaster University, Hamilton, ON, as a Natural Sciences and Engineering Research Council of Canada Postdoctoral Fellow. Since July 2006, he has been with the Department of Electrical and Computer Engineering, University of Manitoba, Winnipeg, MB, Canada, where he is currently a Professor. His current research interests include energy-efficient and green communications, dynamic spectrum management and cognitive radio, radio resource management in wireless communications networks, and performance analysis. He was the TPC Co-Chair for IEEE VTC-Fall 2012 Wireless Applications and Services Track, IEEE Globecom 2010 Wireless Communications Symposium, and IWCMC 2008 General Symposium; the Publicity Co-Chair for IWCMC in 2010, 2011, 2013, and 2014; and the Registration Chair for QShine in 2005. He was also on the editorial board of the *Journal of Computer Systems, Networks, and Communications* and as a Guest Editor of the special issue of the "Association for Computing Machinery Mobile Networks and Applications". He received the Best Paper Award from Chinacom in 2013, the Rh Award for outstanding contributions to research in applied sciences in 2012 from the University of Manitoba, and the Outstanding Service Award from IEEE Globecom in 2010.

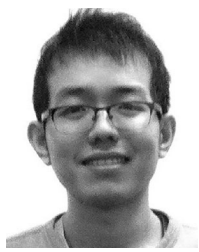

Changyan Yi (S'16–M'18) received the B.Sc. degree from the Guilin University of Electronic Technology, Guilin, China, in 2012, the M.Sc. and Ph.D. degrees from the University of Manitoba, Manitoba, MB, Canada, in 2014 and 2018, respectively. He is currently working as a Research Associate with the Electrical and Computer Engineering, Department, University of Manitoba, Canada. His research interests include algorithmic game theory, queueing theory and their applications in radio resource management, wireless transmission scheduling and network economics. He was awarded Chinese Government Award for Outstanding Students Abroad in 2017, A. Keith Dixon Graduate Scholarship in Engineering for 2017–2018, Edward R. Toporeck Graduate Fellowship in Engineering for 2014–2017 (four times), University of Manitoba Graduate Fellowship (UMGF) for 2015–2018, and IEEE ComSoc Student Travel Grant for IEEE Globecom 2016.